



# COM DEV LTD.

EXECUTIVE SUMMARY TO FINAL REPORT

DEVELOPMENT OF MICROSTRIP ANTENNA  
TECHNOLOGY FOR THE CANADIAN  
MSAT PROGRAMME

TDE/MST/2500/001

PROJECT 2500



- MICROWAVE PRODUCTS
- CONSULTING SERVICES

IC

LKC  
P  
91  
.C654  
D49  
1986  
Summ.

155 SH

E, CAMBRIDGE, ONTARIO, CANADA N1R 7H6 • TEL.: (519) 622-2300 • TWX: 610-366-3164



RELEASABLE

DOC-CR-SP-86-033

# REVISION RECORD

LTR

ECN

NUMBER

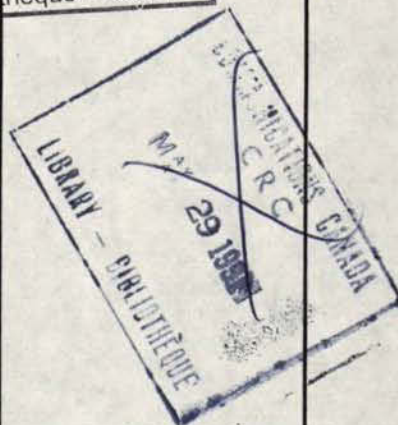
APPD

DATE

Industry Canada  
Library - Queen

AUG 14 2012

Industrie Canada  
Bibliothèque - Queen



WRITTEN

DATE

*Stephen J. Kavanagh*  
7/3/86

CHECKED

DATE

*W. Kavanagh*  
8/11/86

APPROVED

DATE

*W. Kavanagh*  
8/11/86



COM DEV

155 Sheldon Drive  
Cambridge, Ontario  
Canada N1R 7H6

EXECUTIVE SUMMARY TO  
FINAL REPORT  
DEVELOPMENT OF MICROSTRIP ANTENNA  
TECHNOLOGY FOR THE CANADIAN  
MSAT PROGRAMME

DOCUMENT No.

REV.

TDE/MST/2500/001

MSAT  
PROJECT #2500

SHEET 1 OF 81

© Her Majesty the Queen in Right of Canada (1986) as  
represented by the Minister of Supply And Services.

PD 7067526  
DL 10585232  
P91  
C034  
D4863  
1986  
S-cha

# TABLE OF CONTENTS

| <u>ITEM</u> | <u>DESCRIPTION</u>   | <u>PAGE</u> |
|-------------|--|-------------|
| 1.0         | INTRODUCTION   | 7           |
| 2.0         | ANTENNA REQUIREMENTS FOR MSAT                                    | 8           |
| 2.1         | Background   | 8           |
| 2.2         | Reflector Antenna Systems  | 8           |
| 2.2.1       | Two Beam Configuration   | 8           |
| 2.2.2       | Four Beam Configuration  | 9           |
| 2.3         | Direct Radiating Arrays  | 10          |
| 3.0         | PATCH ANTENNA ELEMENTS   | 18          |
| 3.1         | Microstrip Patch Radiators                                       | 18          |
| 3.1.1       | Description  | 18          |
| 3.2         | Single Band Patch Antenna Experiments                            | 18          |
| 3.3         | Experiments with Stacked Patch Antennas                          | 21          |
| 3.3.1       | Experimental Antennas  | 21          |
| 3.3.2       | Characteristic of Stacked Air-Dielectric<br>Square Patch Antenna | 31          |
| 3.3.3       | Mutual Coupling Between Stacked Patch Antennas                   | 39          |
| 3.4         | Power Handling Capability of Patch Elements                      | 48          |
| 4.0         | BEAM FORMING NETWORK TECHNOLOGY                                  | 50          |
| 4.1         | Transmission Line Options  | 50          |
| 4.2         | Experimental Coupler Design                                      | 51          |
| 4.3         | Recommendations for BFN Development                              | 51          |



## TABLE OF CONTENTS

| <u>ITEM</u> | <u>DESCRIPTION</u>               | <u>PAGE</u> |
|-------------|----------------------------------|-------------|
| 5.0         | DESCRIPTION OF ENGINEERING MODEL | 59          |
| 5.1         | Construction                     | 59          |
| 5.2         | RF Performance                   | 64          |
| 6.0         | CONCLUSIONS                      | 79          |

## LIST OF TABLES

| <u>ITEM</u> | <u>DESCRIPTION</u>   | <u>PAGE</u> |
|-------------|--|-------------|
| TABLE 2.1   | LOSS BUDGET ESTIMATE FOR 2-BEAM ARRAY                                      | 11          |
| TABLE 3.1   | MEASURED CHARACTERISTICS OF BREADBOARD SINGLE<br>BAND PATCH ELEMENTS       | 22          |
| TABLE 3.2   | BEAMWIDTHS AND SQUINT OF BREADBOARD SINGLE<br>BAND PATCH ELEMENTS          | 23          |
| TABLE 3.3   | RETURN LOSS AND ISOLATION SUMMARY FOR<br>BREADBOARD STACKED PATCH ANTENNA  | 38          |
| TABLE 3.4   | BEAMWIDTHS AND SQUINT OF BREADBOARD<br>STACKED PATCH ELEMENT               | 42          |
| TABLE 3.5   | MUTUAL COUPLING BETWEEN STACKED PATCH<br>ANTENNAS IN SEPTET CONFIGURATIONS | 47          |
| TABLE 5.1   | ENGINEERING MODEL RETURN LOSS AND ISOLATION<br>SUMMARY                     | 60          |
| TABLE 5.2   | ENGINEERING MODEL PATTERN SUMMARY  | 78          |

# LIST OF FIGURES

| <u>ITEM</u> | <u>DESCRIPTION</u>  | <u>PAGE</u> |
|-------------|---|-------------|
| FIGURE 2.1  | TWO BEAM FEED ARRAY FOR 4.9m REFLECTOR  | 12          |
| FIGURE 2.2  | COMPUTED DIRECTIVITY CONTOURS OF 4.9m REFLECTOR<br>WITH 10 ELEMENT 2-BEAM MICROSTRIP FEED ARRAY<br>AT 823 MHz       | 13          |
| FIGURE 2.3  | COMPUTED DIRECTIVITY CONTOURS OF 4.9m REFLECTOR<br>WITH 10 ELEMENT 2-BEAM MICROSTRIP FEED ARRAY AT<br>868 MHz       | 14          |
| FIGURE 2.4  | FOUR BEAM FEED ARRAY FOR 7.3m REFLECTOR   | 15          |
| FIGURE 2.5  | COMPUTED 29 dB DIRECTIVITY CONTOURS OF 7.3m<br>REFLECTOR WITH 21 ELEMENT 4-BEAM MICROSTRIP FEED<br>ARRAY AT 823 MHz | 16          |
| FIGURE 2.6  | COMPUTED 29 dB DIRECTIVITY CONTOURS OF 7.3m<br>REFLECTOR WITH 21 ELEMENT 4-BEAM MICROSTRIP FEED<br>ARRAY AT 868 MHz | 17          |
| FIGURE 3.1  | TYPICAL MICROSTRIP ANTENNAS   | 19          |
| FIGURE 3.2  | SINGLE PATCH ANTENNA WITH TWO FEEDS (SINGLE BAND<br>BREADBOARD)   | 20          |
| FIGURE 3.3  | MEASURED RETURN LOSS AND ISOLATION OF BREADBOARD<br>RECEIVE BAND ELEMENT (INPUT TO PORT 1)                          | 24          |
| FIGURE 3.4  | MEASURED RETURN LOSS AND ISOLATION OF BREADBOARD<br>RECEIVE BAND ELEMENT (INPUT TO PORT 2)                          | 25          |
| FIGURE 3.5  | MEASURED RETURN LOSS AND ISOLATION OF BREADBOARD<br>TRANSMIT BAND ELEMENT (INPUT TO PORT 1)                         | 26          |
| FIGURE 3.6  | MEASURED RETURN LOSS AND ISOLATION OF BREADBOARD<br>TRANSMIT BAND ELEMENT (INPUT TO PORT 2)                         | 27          |
| FIGURE 3.7  | MEASURED E- AND H-PLANE PATTERNS OF BREADBOARD<br>RECEIVE BAND ELEMENT AT 823 MHz                                   | 28          |
| FIGURE 3.8  | MEASURED E- AND H-PLANE PATTERNS OF BREADBOARD<br>TRANSMIT BAND ELEMENT AT 868 MHz                                  | 29          |
| FIGURE 3.9  | EXPERIMENTAL STACKED PATCH ANTENNA  | 30          |
| FIGURE 3.10 | EQUIVALENT CIRCUIT FOR STACKED PATCH ANTENNA  | 32          |





# LIST OF FIGURES

| <u>ITEM</u> | <u>DESCRIPTION</u>  | <u>PAGE</u> |
|-------------|---|-------------|
| FIGURE 3.11 | RETURN LOSS AND BANDWIDTH OF STACKED<br>PATCH ANTENNAS  | 33          |
| FIGURE 3.12 | RETURN LOSS AND ISOLATION OF A STACKED AIR-<br>DIELECTRIC SQUARE PATCH ANTENNA                                    | 35          |
| FIGURE 3.13 | MEASURED RETURN LOSS AND PORT-TO-PORT ISOLATION<br>OF BREADBOARD STACKED PATCH ANTENNA (INPUT TO<br>PORT 1)       | 36          |
| FIGURE 3.14 | MEASURED RETURN LOSS AND PORT-TO-PORT ISOLATION<br>OF BREADBOARD STACKED PATCH ANTENNA (INPUT TO<br>PORT 2)       | 37          |
| FIGURE 3.15 | MEASURED E- AND H-PLANE PATTERNS OF BREADBOARD<br>STACKED PATCH ELEMENT AT 823 MHz                                | 40          |
| FIGURE 3.16 | MEASURED E- AND H-PLANE PATTERNS OF BREADBOARD<br>STACKED PATCH ELEMENT AT 868 MHz                                | 41          |
| FIGURE 3.17 | GEOMETRY OF E- AND H-PLANE MUTUAL COUPLING  | 43          |
| FIGURE 3.18 | MEASURED E- AND H-PLANE MUTUAL COUPLING VERSUS<br>SPACING BETWEEN BREADBOARD STACKED PATCH ANTENNAS<br>AT 820 MHz | 44          |
| FIGURE 3.19 | MEASURED E- AND H-PLANE MUTUAL COUPLING VERSUS<br>SPACING BETWEEN BREADBOARD STACKED PATCH ANTENNAS<br>AT 870 MHz | 45          |
| FIGURE 3.20 | SEPTET COUPLING GEOMETRIES (VIEWED TOWARD FRONT<br>FACE, ALL CASES 12 IN. CENTRE-TO-CENTRE SPACING)               | 46          |
| FIGURE 4.1  | MEASURED RETURN LOSS OF STRIPLINE COUPLER   | 52          |
| FIGURE 4.2  | MEASURED ISOLATION OF STRIPLINE COUPLER   | 53          |
| FIGURE 4.3  | MEASURED STRAIGHT-THROUGH LOSS OF STRIPLINE<br>COUPLER  | 54          |
| FIGURE 4.4  | MEASURED COUPLING OF STRIPLINE COUPLER  | 55          |
| FIGURE 4.5  | TOTAL LOSS OF EXPERIMENTAL STRIPLINE COUPLER  | 56          |



# LIST OF FIGURES

| <u>ITEM</u> | <u>DESCRIPTION</u>  | <u>PAGE</u> |
|-------------|---|-------------|
| FIGURE 5.1  | ENGINEERING MODEL EXPLODED VIEW   | 61          |
| FIGURE 5.2  | PHOTOGRAPH OF ENGINEERING MODEL DURING<br>ASSEMBLY SHOWING BFN LAYER              | 65          |
| FIGURE 5.3  | PHOTOGRAPH OF ENGINEERING MODEL DURING<br>ASSEMBLY SHOWING COUPLER LAYER          | 66          |
| FIGURE 5.4  | PHOTOGRAPH OF ENGINEERING MODEL<br>BEFORE PATCH ASSEMBLY                          | 67          |
| FIGURE 5.5  | COMPLETED ENGINEERING MODEL   | 68          |
| FIGURE 5.6  | FRONT FACE OF COMPLETED ENGINEERING<br>MODEL MOUNTED IN GROUND PLANE<br>EXTENSION | 69          |
| FIGURE 5.7  | BACK FACE OF COMPLETED ENGINEERING MODEL<br>MOUNTED IN GROUND PLANE EXTENSION     | 70          |
| FIGURE 5.8  | RETURN LOSS AND ISOLATION OF ENGINEERING<br>MODEL ELEMENT (INPUT TO PORT 1)       | 71          |
| FIGURE 5.9  | RETURN LOSS AND ISOLATION OF ENGINEERING<br>MODEL ELEMENT (INPUT TO PORT 2)       | 72          |
| FIGURE 5.10 | E-AND H-PLANE PATTERNS OF ENGINEERING MODEL<br>ELEMENT AT 823 MHz (PORT 1)        | 73          |
| FIGURE 5.11 | E- AND H-PLANE PATTERNS OF ENGINEERING MODEL<br>ELEMENT AT 823 MHz (PORT 2)       | 74          |
| FIGURE 5.12 | E-AND H-PLANE PATTERNS OF ENGINEERING MODEL<br>ELEMENT AT 868 MHz (PORT 1)        | 75          |
| FIGURE 5.13 | E-AND H-PLANE PATTERNS OF ENGINEERING MODEL<br>ELEMENT AT 868 MHz (PORT 2)        | 76          |



INTRODUCTION

The first generation MSAT system concept uses one satellite covering North America using transmit and receive frequencies in the UHF band (near 850 MHz) for communication with mobile stations. One or more large deployable reflectors (in the 4-9 metre diameter range) have been suggested as antennas capable of sufficient gain to minimize the size and cost of the mobile station antennas. A multibeam feed producing a small number of beams (typically 2-4) may be used. If conventional horn antennas are used in this feed the mass and volume of the feed may be excessive.

Microstrip antennas offer an alternative technology which because of their planar geometry have the potential to reduce the mass and volume requirements of the feed array. Their major drawbacks are narrow bandwidth and a lack of previously developed techniques for space applications. The primary goal of this study has been to investigate the use of a microstrip antenna feed capable of simultaneous transmit and receive operation in both right and left hand circular polarization. This could, in principle, permit the use of a single reflector at UHF.

This executive summary report contains a review of system requirements and of microstrip antenna technology, especially with regard to dual band or wideband radiators. The results of a program of development of suitable patch antenna elements and some of the necessary beam-forming network components are described.

## 2.0 ANTENNA REQUIREMENTS FOR MSAT

### 2.1 Background

A variety of system concepts for mobile communications satellites have been proposed, using either UHF frequencies (near 850 MHz) or L-Band (near 1.5 GHz), or both. Most specify coverage of CONUS and Canada and some include Alaska. Primarily because of limitations on antenna size a small number of beams is used.

We have chosen to consider the use of microstrip antennas to provide similar performance to two and four beam UHF configurations proposed by SPAR Aerospace. SPAR's 2 beam design does not cover all of Alaska and achieves an edge of coverage directivity of 28 dB using a 4.9m diameter reflector with both beams having the same polarization and no frequency reuse. Circular polarization is used. Their four beam design includes coverage of Alaska and has 29 dB directivity at the edge of coverage, using a 7.3m diameter reflector. There is frequency reuse in the easternmost and westernmost beams. In both designs all beams have the same sense of polarization. A satellite located at 109° west is assumed. This section describes the use of microstrip array fed reflectors and direct radiating microstrip arrays to provide similar levels of service.

### 2.2 Reflector Antenna Systems

#### 2.2.1 Two Beam Configuration

To form two overlapping beams for both transmit and receive, there are a number of options available to trade between the number of reflectors, feed complexity and earth station requirements.





For this study the single reflector case was chosen for most of the analysis as it is potentially the most difficult and any results can be applied to the other configurations quite easily. The same reflector diameter as the SPAR design (4.9m) was chosen. It is mounted on the east side of the spacecraft and offset along the east/west axis. The two beams are of opposite senses of circular polarization. The feed array is composed of a triangular grid of square patch elements with 12 inch spacing between centres. The array contains two overlapping septets of patches for a total of 10 elements as shown in Figure 2.1. Each septet corresponds to a beam. Behind each element is a 3dB coupler to produce circular polarization. Each of the two inputs to this coupler produces one of the two senses of polarization.

The calculated directivity contours for this 10 element feed and 4.9m reflector are shown in Figures 2.2 (823 MHz) and 2.3 (868 MHz). The circular beams are very similar in performance to the SPAR design. No frequency reuse is possible as the cross-polar levels are too high for such closely spaced beams.

#### 2.2.2 Four Beam Configuration

Similar options to the two beam case are available in choosing the number of reflectors and the feed systems for a four beam configuration. Again the single reflector with beams of alternating sense of polarization was chosen. The feed array is a 12 inch spaced triangular grid of square vacuum-dielectric patch elements and is used with a 7.3m diameter reflector (same as SPAR) with an f/D ratio of 0.85. A total of 21 elements are required, as shown in Figure 2.4. The computed 29dB directivity contours are shown in Figures 2.5 (823 MHz) and 2.6 (868 MHz). Computation of interference levels between the eastern most and western most beams have been carried out to evaluate the feasibility of frequency reuse. Co-polarized interference is at

least 45 dB below the desired signal but cross-polarized interference is in some areas only about 20 dB down.

### 2.3 Direct Radiating Arrays

While considering the feasibility of using direct radiating microstrip arrays for MSAT, effort has been concentrated on obtaining comparable beam plans and performance to the reflector configurations discussed above.

While the array is slightly smaller than the reflector and does not require the extra focal length dimension it will be substantially heavier if high performance is to be maintained.

An attempt to define a single array to produce a 4-beam footprint similar to that of the 7.3 m reflector was not successful. This is a result of the characteristics of orthogonal beams. Only two arbitrary beams may be generated by one array as described above.

Surprisingly, microstrip arrays, which are often considered as light weight, low cost antennas appear inferior to reflectors in this application. In fact such arrays are more suited to antennas requiring a large number of beams or especially wide angle scanning. The low loss, high power beamformers and beam plans with large overlaps pose serious difficulties for such antennas for use on MSAT.



TABLE 2.1 LOSS BUDGET ESTIMATE FOR 2-BEAM ARRAY

|                                       | <u>LOSS</u> |
|---------------------------------------|-------------|
| Loss in patch element                 | 0.1 dB      |
| CP coupler loss                       | 0.09        |
| BFN Coupler Losses: 8 at 0.09 dB each | 0.72        |
| Stripline: 2 m at 0.25 dB/m           | 0.50        |
| Patch return loss: 20 dB              | 0.05        |
| Input return loss: 20 dB              | 0.05        |
|                                       | <hr/>       |
| TOTAL                                 | 1.51 dB     |

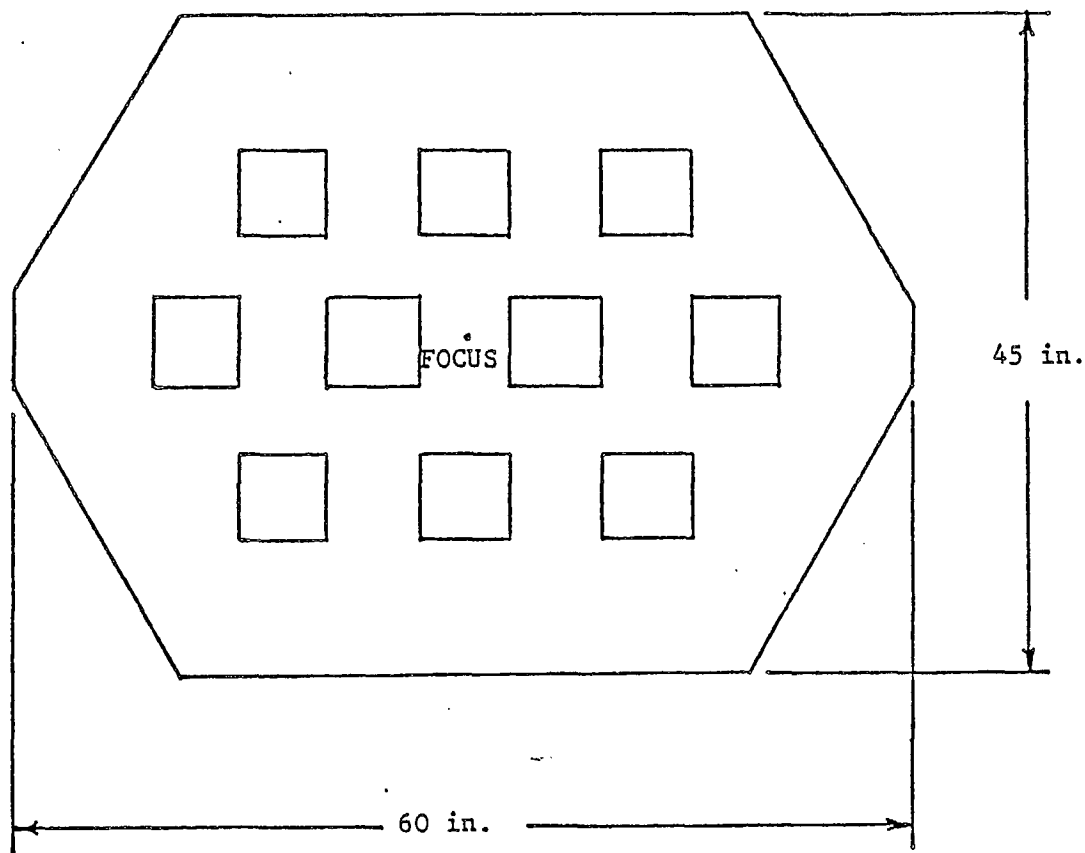


FIGURE 2.1: TWO BEAM FEED ARRAY FOR 4.9 m REFLECTOR

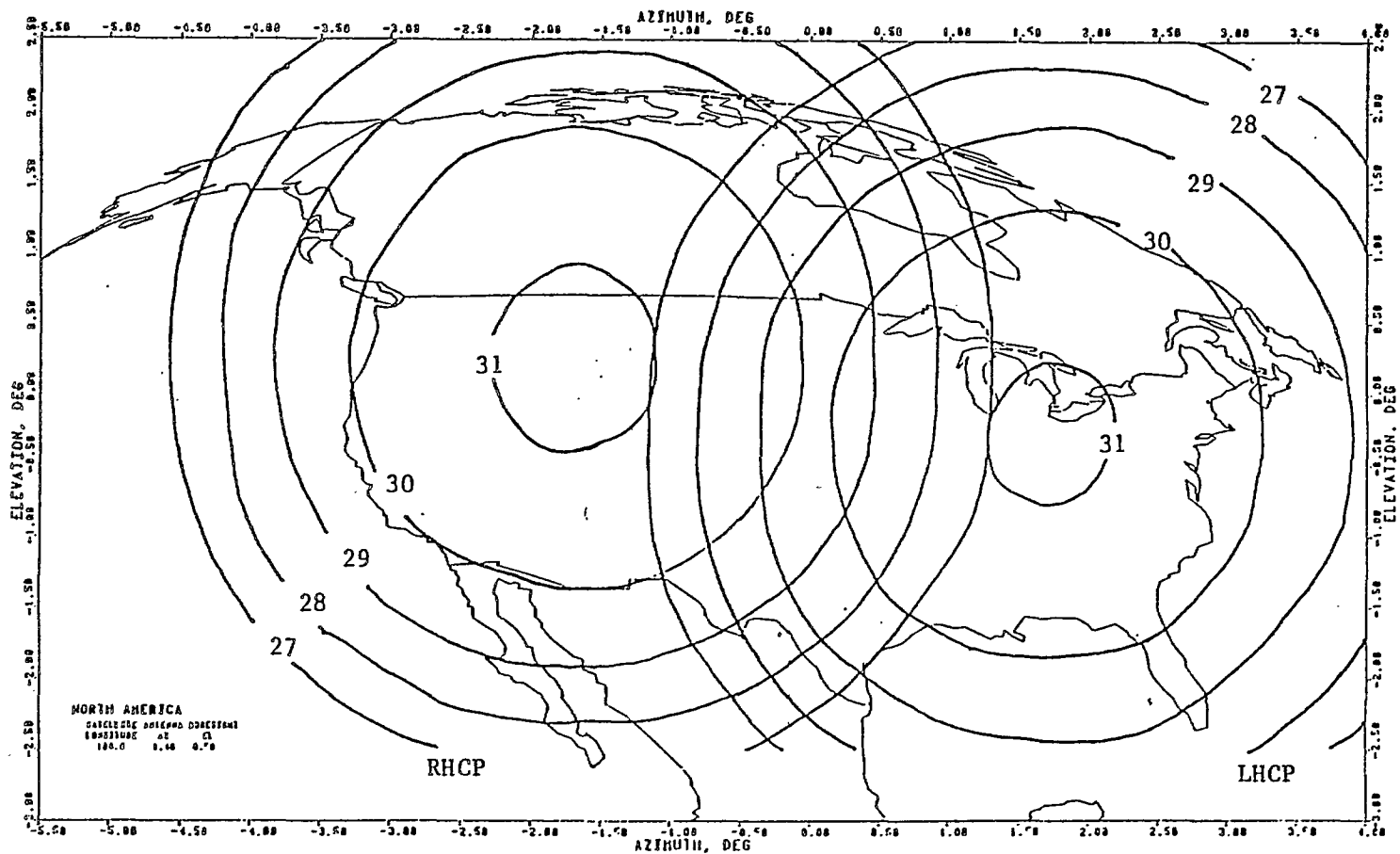


FIGURE 2.2: COMPUTED DIRECTIVITY CONTOURS OF 4.9 m REFLECTOR WITH 10 ELEMENT 2-BEAM MICROSTRIP FEED ARRAY AT 823 MHz

DOCUMENT NO.

REV.

TIDE/MST/2500/001

**COM DEV**

SHEET 13

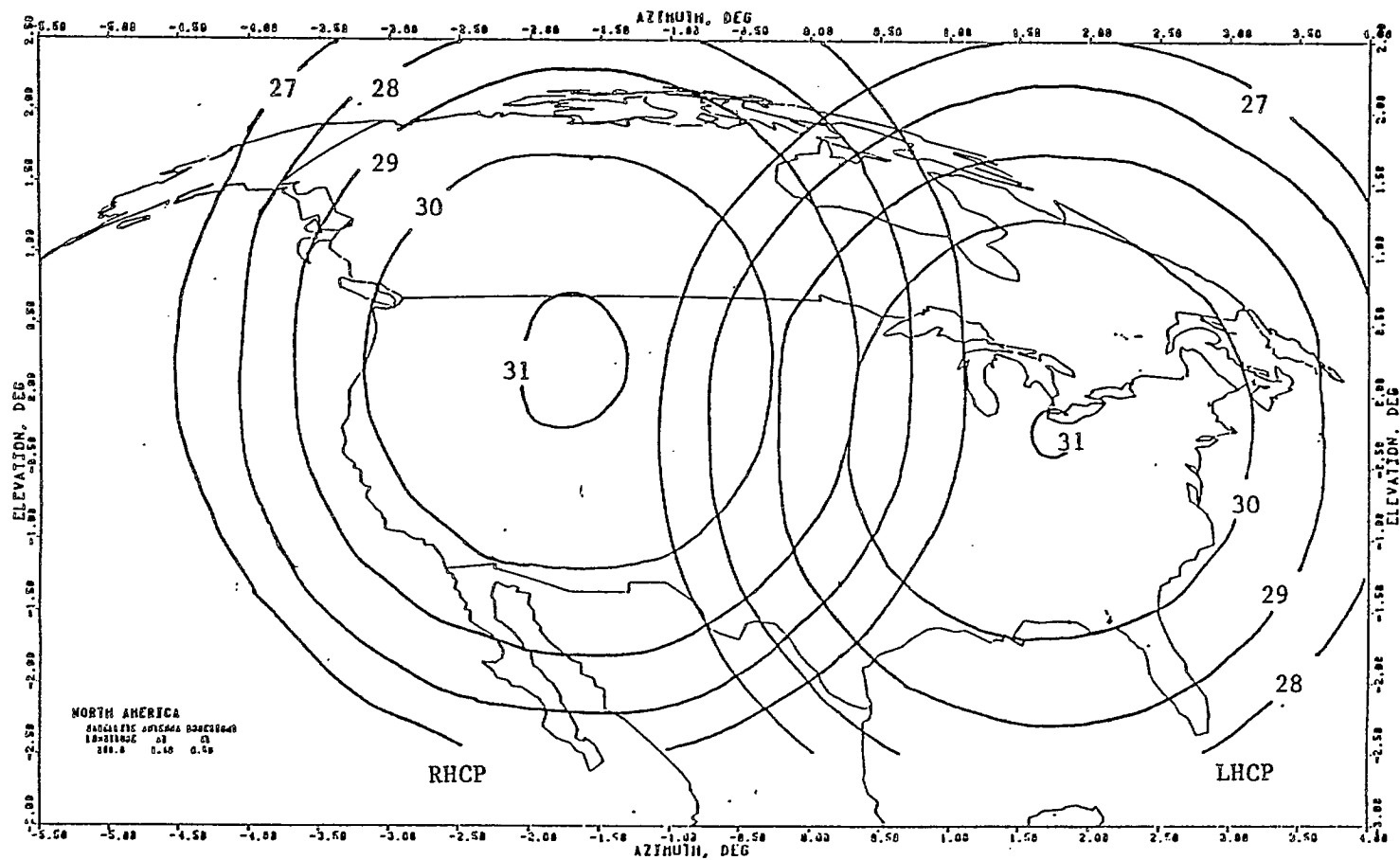


FIGURE 2.3: COMPUTED DIRECTIVITY CONTOURS OF 4.9 m REFLECTOR WITH 10 ELEMENT 2-BEAM MICROSTRIP FEED ARRAY AT 868 MHz

DOCUMENT NO.

REV.

TDE/MST/2500/001

SHEET

14

**COM DEV**

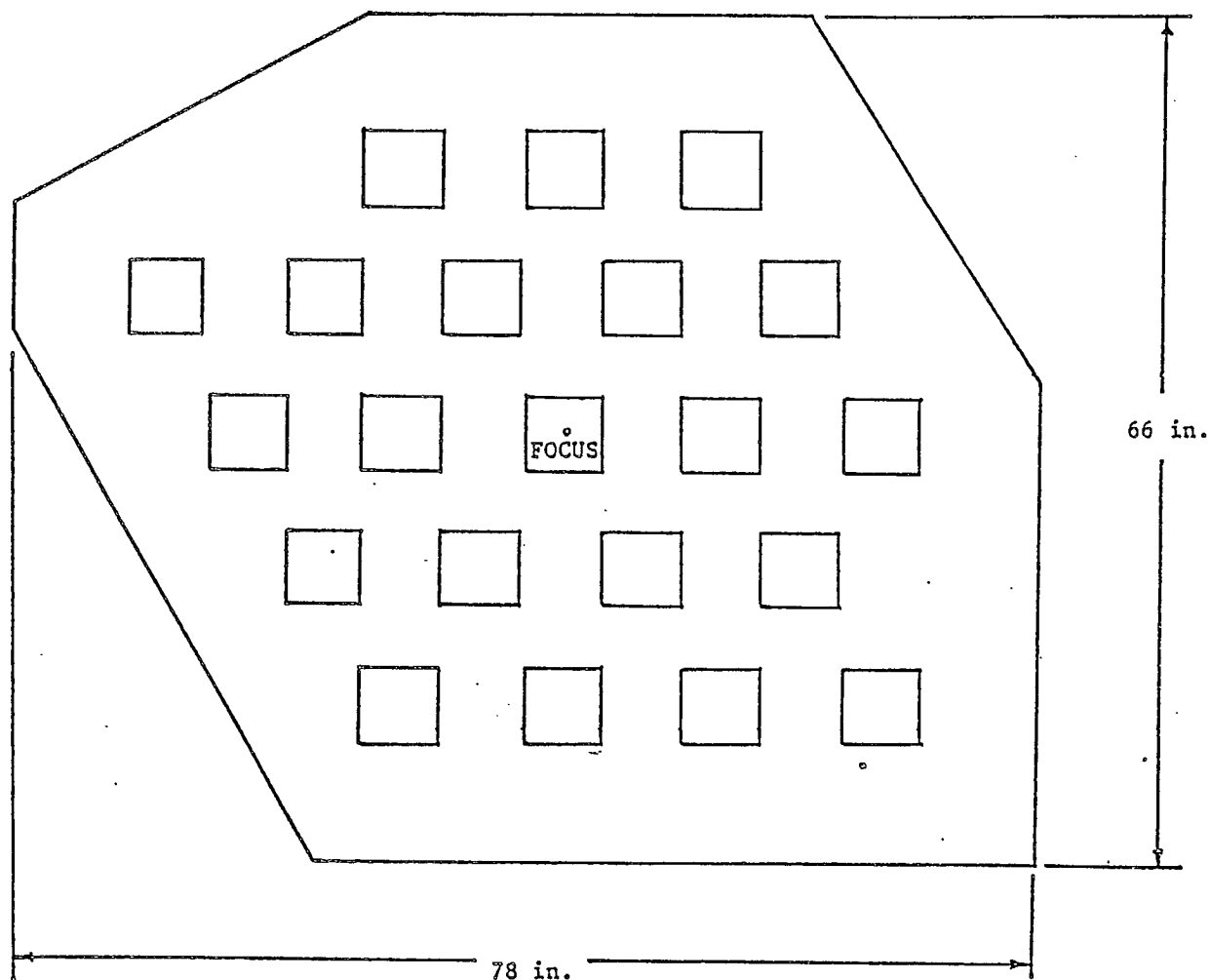


FIGURE 2.4: FOUR BEAM FEED ARRAY FOR 7.3 m REFLECTOR



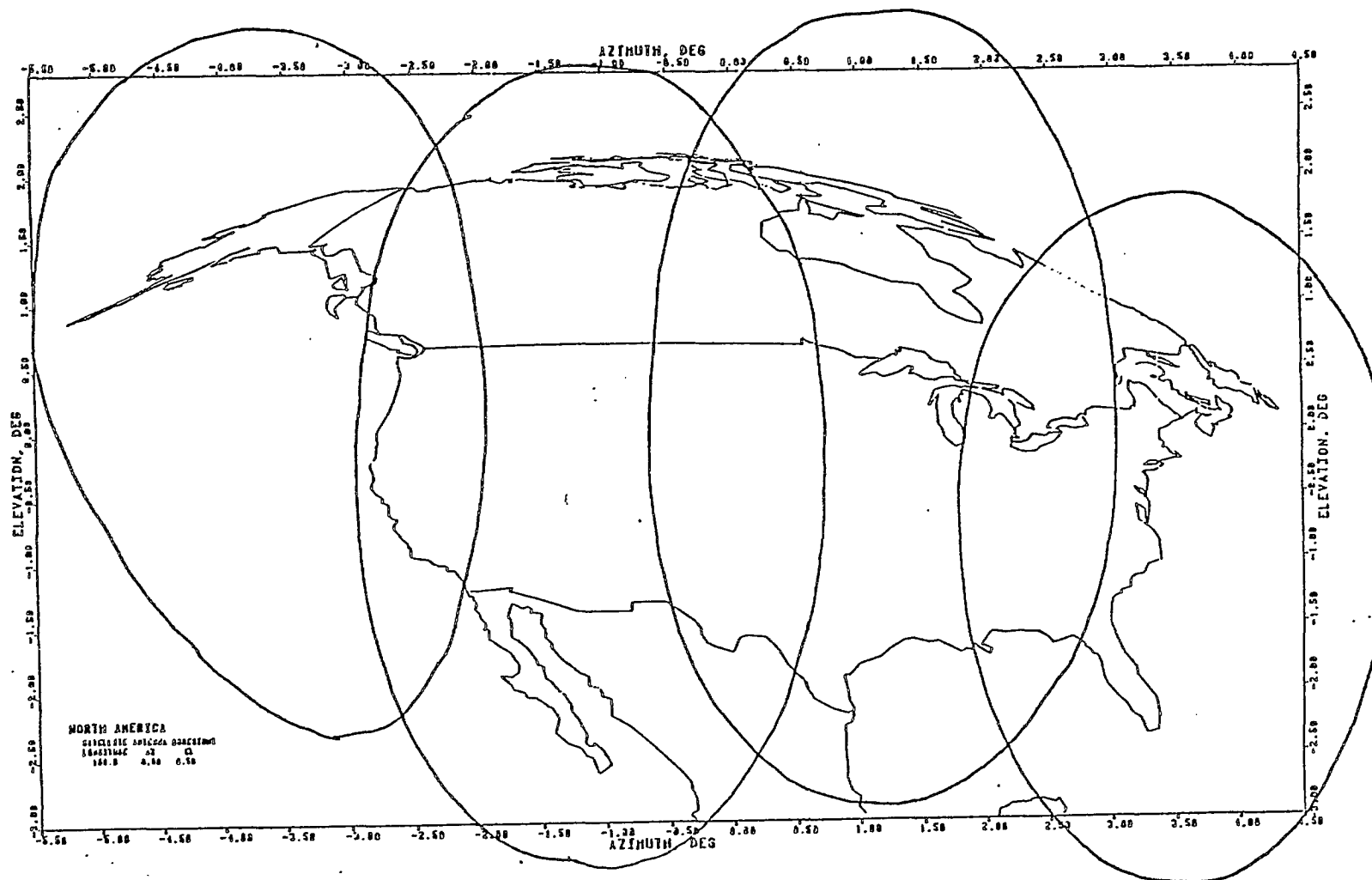


FIGURE 2.5: COMPUTED 29 dB DIRECTIVITY CONTOURS OF 7.3 m REFLECTOR WITH 21 ELEMENT 4-BEAM MICROSTRIP FEED ARRAY AT 823 MHz

DOCUMENT NO.

REV.

TDE/MST/2500/001



COM DEV

SHEET 16

Her Majesty the Queen in Right of Canada (1986) as represented by the Minister of Supply And Services.

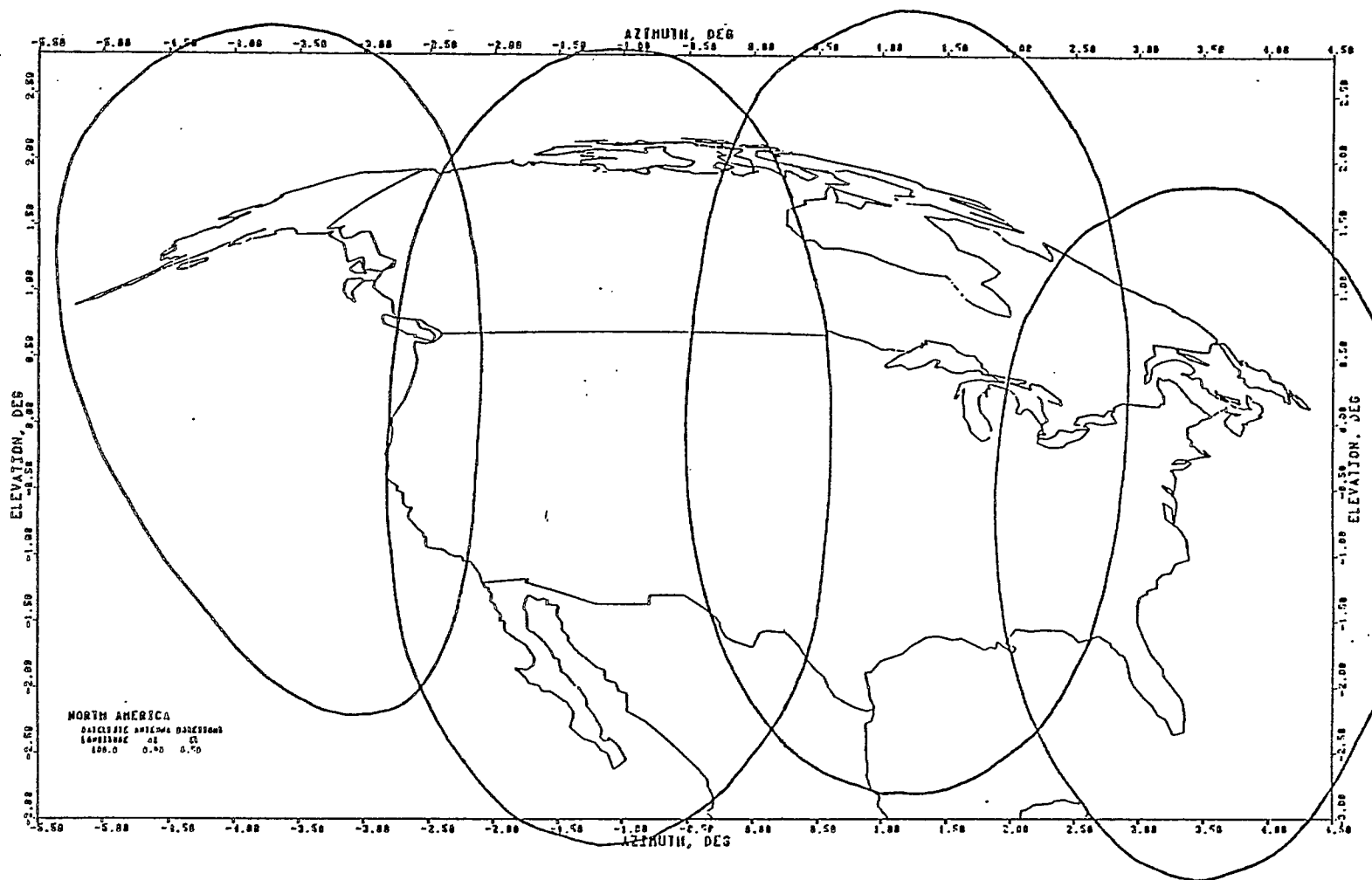


FIGURE 2.6: COMPUTED 29 dB DIRECTIVITY CONTOURS OF 7.3 m REFLECTOR WITH 21 ELEMENT 4-BEAM MICROSTRIP FEED ARRAY AT 868 MHz

DOCUMENT NO.

REV.

TDE/MST/2500/001

**COM DEV**  
SHEET 17

### 3.0 PATCH ANTENNA ELEMENTS

#### 3.1 Microstrip Patch Radiators

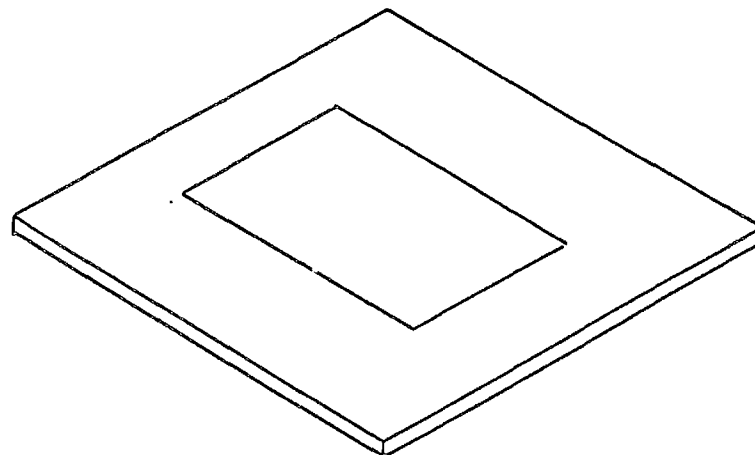
##### 3.1.1 Description

The most common form of microstrip antenna is a patch of metal supported a small distance over a ground plane by a layer of dielectric material. The patch can be any shape although most often it is rectangular or disk-shaped. Frequently the antenna is manufactured by etching the patch on one side of double-sided copper-clad circuit board. It may be fed by a microstrip line etched on the same side of the board as the radiating patch or by a probe extending through the ground plane to circuitry on the back. Some examples of typical microstrip antennas are shown in Figure 3.1. The transverse dimensions of the patch are usually of the order of a half wavelength but the thickness is very much less.

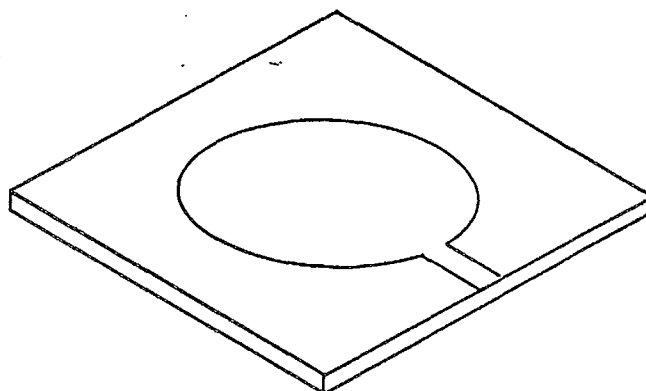
With vacuum dielectric the  $Q$  due to radiation is reduced and the dielectric losses eliminated so a half-inch vacuum spaced patch should lose much less than 0.1 dB due to antenna losses.

#### 3.2 Single Band Patch Antenna Experiments

Different patch sizes were tested to find those with resonances closest to 823 MHz and 868 MHz, the two band centres. The probe positions were optimized for best match. The resulting data was interpolated to find dimensions to obtain matched antennas at 823 MHz and 868 MHz. New antennas with these dimensions were constructed with two orthogonal feeds. The construction of these antennas is shown in Figure 3.2.



RECTANGULAR PATCH WITH COAXIAL PROBE FEED



CIRCULAR PATCH WITH MICROSTRIP LINE FEED

FIGURE 3.1: TYPICAL MICROSTRIP ANTENNAS

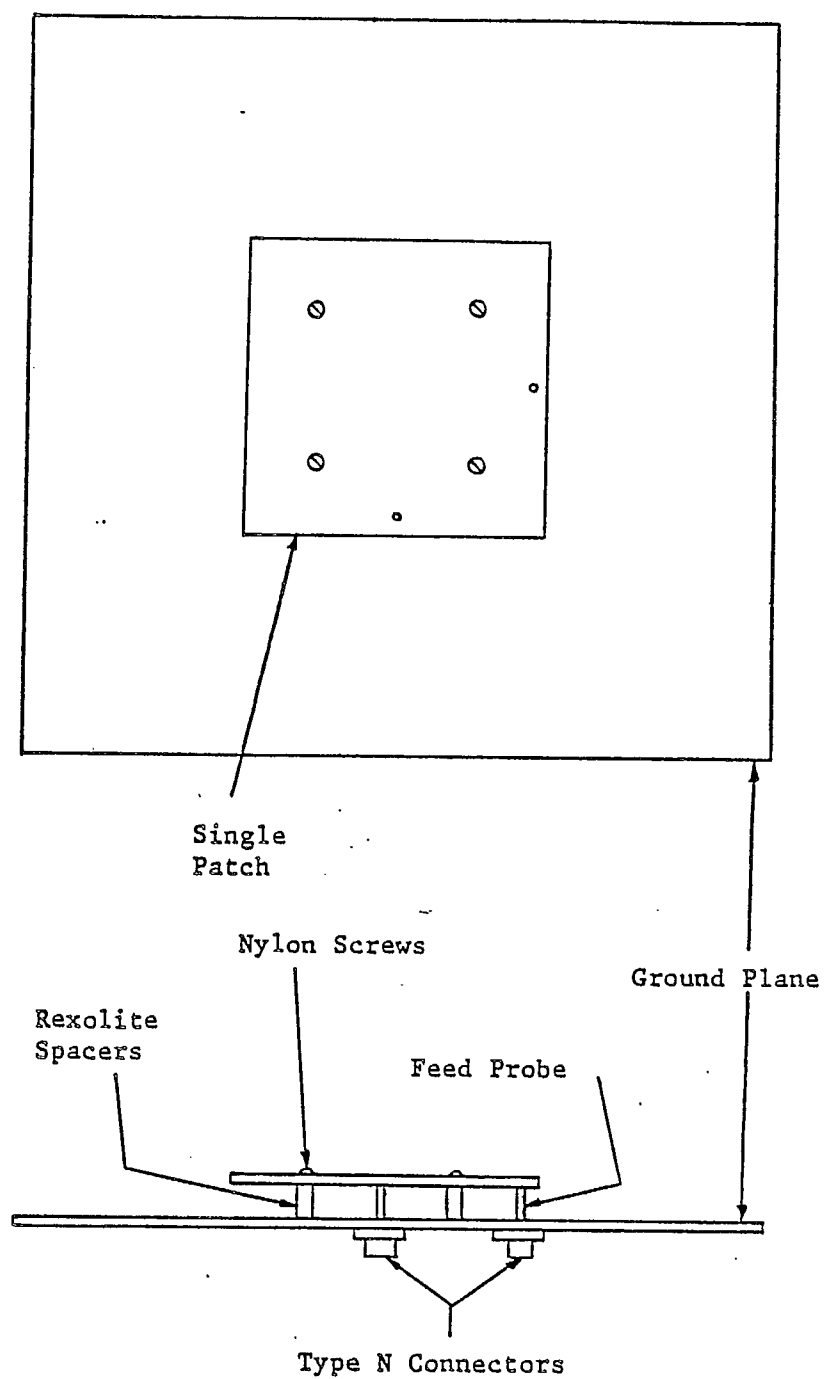


FIGURE 3.2: SINGLE PATCH ANTENNA WITH TWO FEEDS  
(SINGLE BAND BREADBOARD)



In Figures 3.3 to 3.6 are plotted the return losses and port-to-port isolations of these antennas. The isolation is simply the attenuation measured when a signal is applied to one feed port and detected at the other. These tests were done with the patch at the centre of a 30 by 36 inch ground plane. The 823 MHz antenna actually achieves the best match at 820.2 MHz at one port and 821.0 MHz at the other. The 868 MHz patch was resonant at 866.0 MHz at one port and 867.8 MHz at the other. In all cases the 4 MHz MSAT bands were covered with better than 20 dB return loss but the desired thermal contraction/expansion allowance was not covered by every one. One more iteration of the dimensions would permit better centering of the resonant frequencies, but to be truly useful this should be carried out in the array environment in which the element would be used. The isolation in all cases was more than 25 dB. A summary of the measured port characteristics is given in Table 3.1.

Measured E- and H-plane radiation patterns are shown in Figures 3.7 (823 MHz) and 3.8 (868 MHz). The patterns show H-plane patterns somewhat wider than the E-plane patterns. Table 3.2 summarizes radiated characteristics.

### 3.3 Experiments with Stacked Patch Antennas

#### 3.3.1 Experimental Antennas

An empirical study of the characteristics of some stacked patch antennas was carried out as part of this study. Square patches were chosen in order to simplify theoretical analysis.

The experimental antennas were constructed as shown in Figure 3.9. The two patches were made of .06 inch thick brass and were supported on four sets of Rexolite spacers slipped over nylon screws. The parametric study was done using a 24 inch square ground plane with slots cut to permit sliding the feed probe to different distances from the edge of the lower patch.

TABLE 3.1 MEASURED CHARACTERISTICS OF BREADBOARD  
SINGLE BAND PATCH ELEMENTS

|  | Receive Element |        | Transmit Element |        |
|--|-----------------|--------|------------------|--------|
|  | Port 1          | Port 2 | Port 1           | Port 2 |
| Nominal Centre Freq. (MHz)             | 823             | 823    | 868              | 868    |
| Measured Centre Freq. (MHz)            | 820.2           | 821.0  | 866.0            | 867.8  |
| Return Loss in 4 MHz MSAT<br>Band (dB) | 20.3            | 21.8   | 22.0             | 23.5   |
| • Return Loss in 1% Band (dB)          | 21.8            | 21.8   | 21.7             | 21.3   |
| Bandwidth at 20 dB Match (%)           | 1.27            | 1.25   | 1.29             | 1.24   |
| Isolation in 4 MHz MSAT<br>Band (dB)   | 25.6            | 25.3   | 26.1             | 25.8   |
| Isolation in 1% Band (dB)              | 25.8            | 25.3   | 26.0             | 25.4   |

TABLE 3.2: BEAMWIDTHS AND SQUINT OF BREADBOARD  
SINGLE BAND PATCH ELEMENTS

|                               | Half-Power Beamwidth<br>(degrees) | Squint<br>(degrees) |
|-------------------------------|-----------------------------------|---------------------|
| Receive element<br>(823 MHz)  |                                   |                     |
| E-plane                       | 63                                | 2.5                 |
| H-plane                       | 66                                | 2.0                 |
| Transmit element<br>(868 MHz) |                                   |                     |
| E-plane                       | 63                                | 5.5                 |
| H-plane                       | 78                                | 0.0                 |

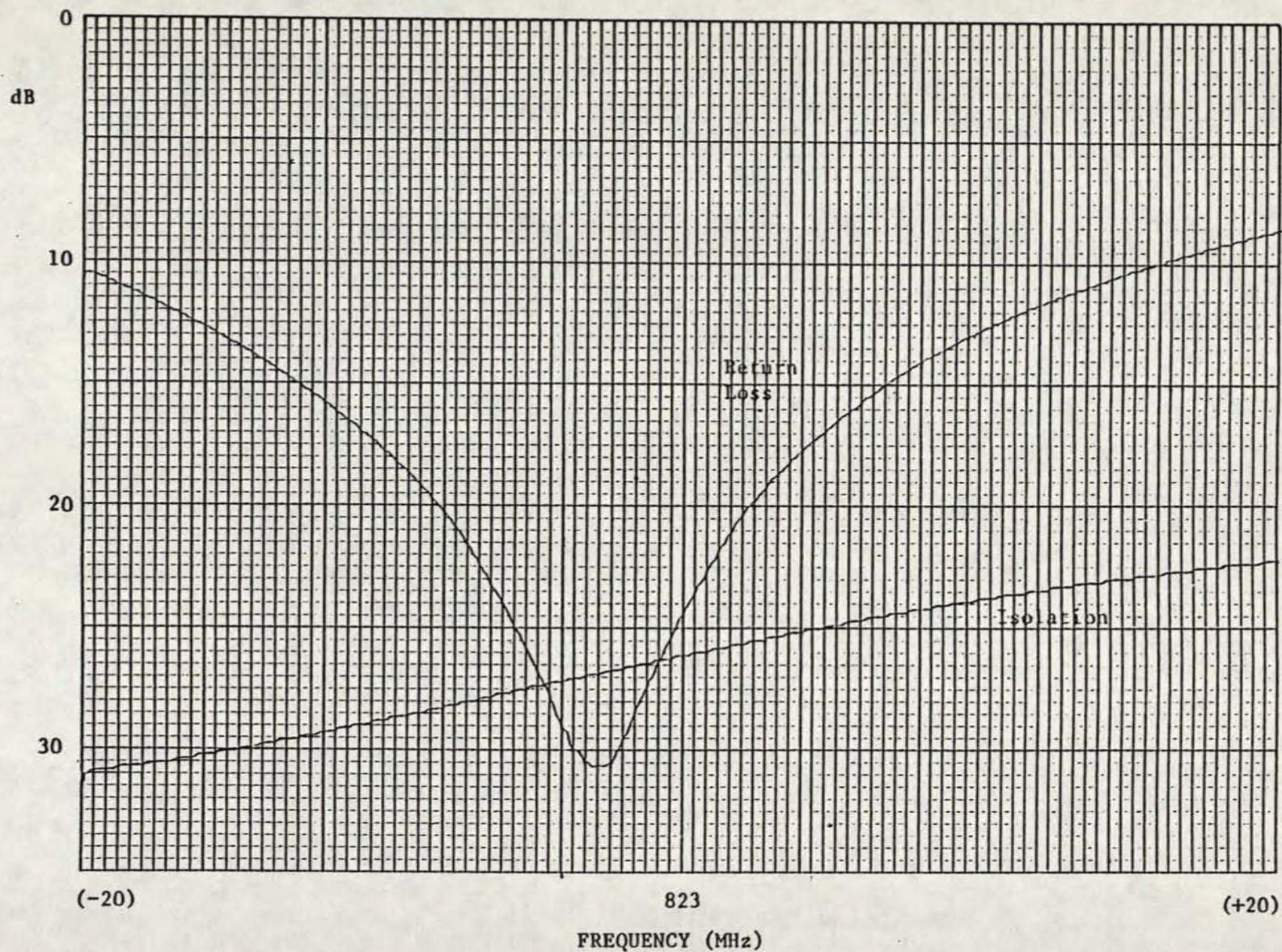


FIGURE 3.3: MEASURED RETURN LOSS AND ISOLATION OF BREADBOARD RECEIVE BAND ELEMENT (INPUT TO PORT 1)

DOCUMENT No.

REV.

TDE/MST/2500/001



COM DEV

SHEET

24



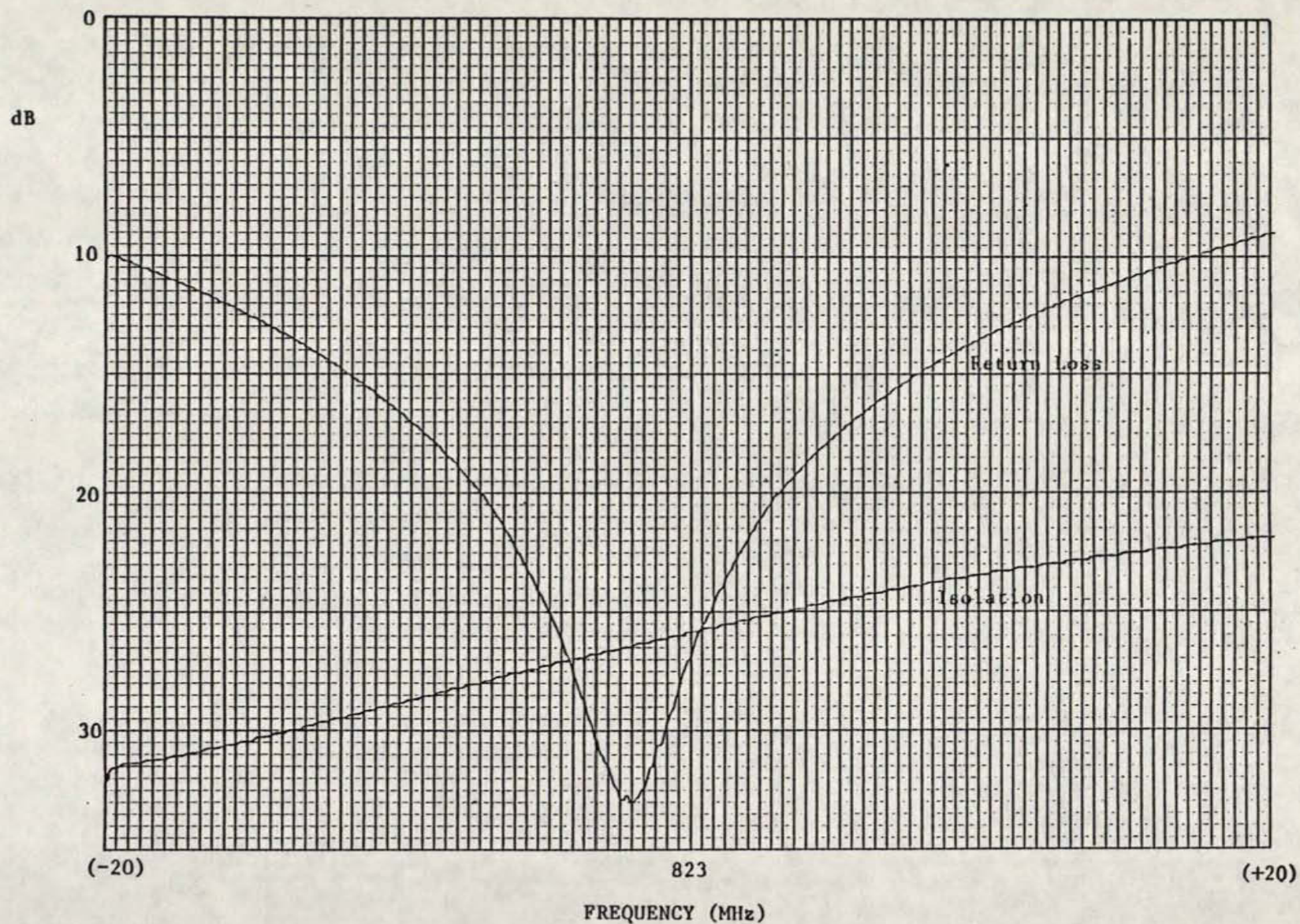


FIGURE 3.4 : MEASURED RETURN LOSS AND ISOLATION OF BREADBOARD RECEIVE BAND ELEMENT (INPUT TO PORT 2)

DOCUMENT NO.

TDE/MST/2500/001

REV.

—



COM DEV

SHEET 25



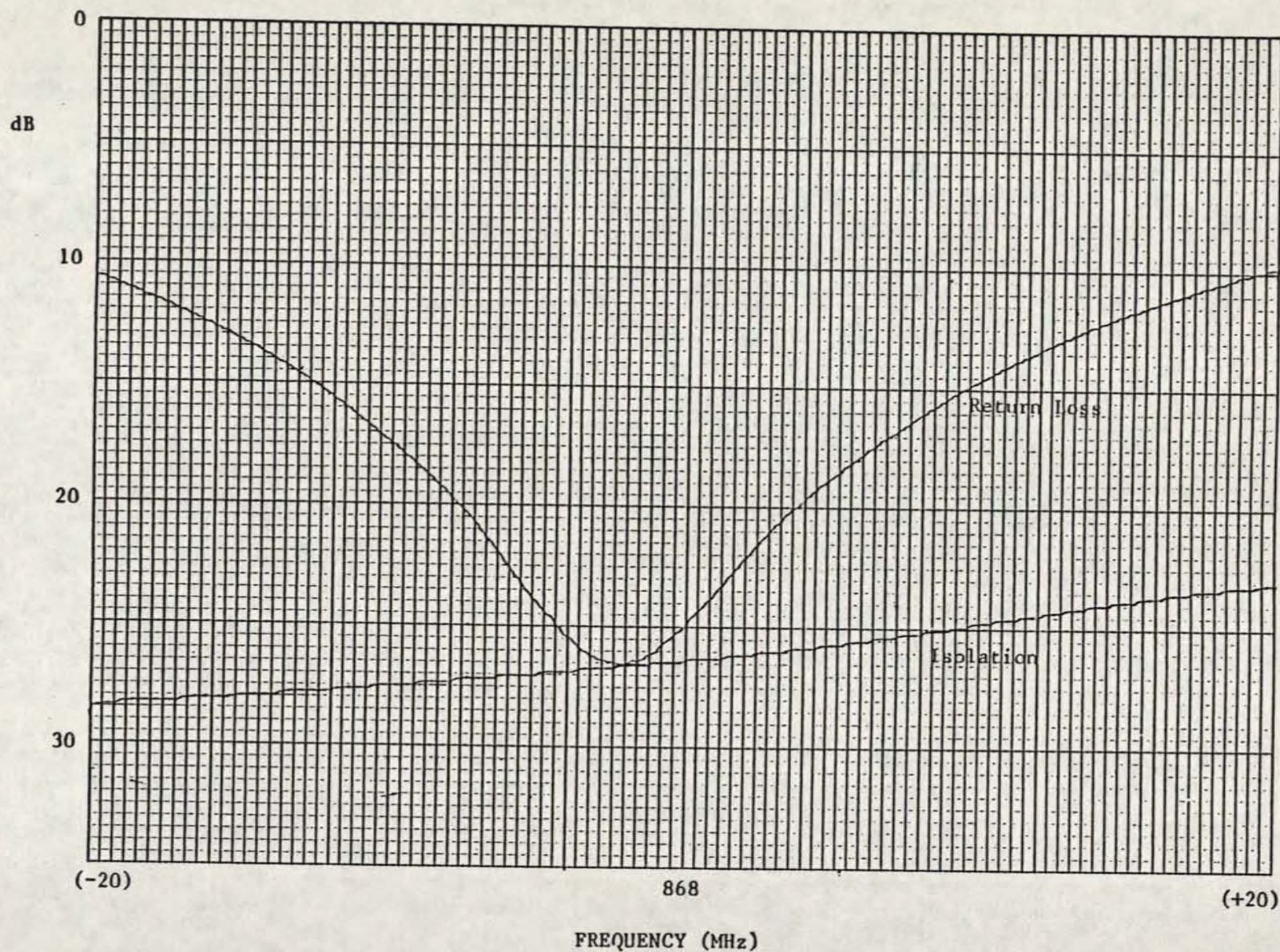


FIGURE 3.5: MEASURED RETURN LOSS AND ISOLATION OF BREADBOARD TRANSMIT BAND ELEMENT (INPUT TO PORT 1)

DOCUMENT NO.

REV.

TDE/MST/2500/001



COM DEV

SHEET 26



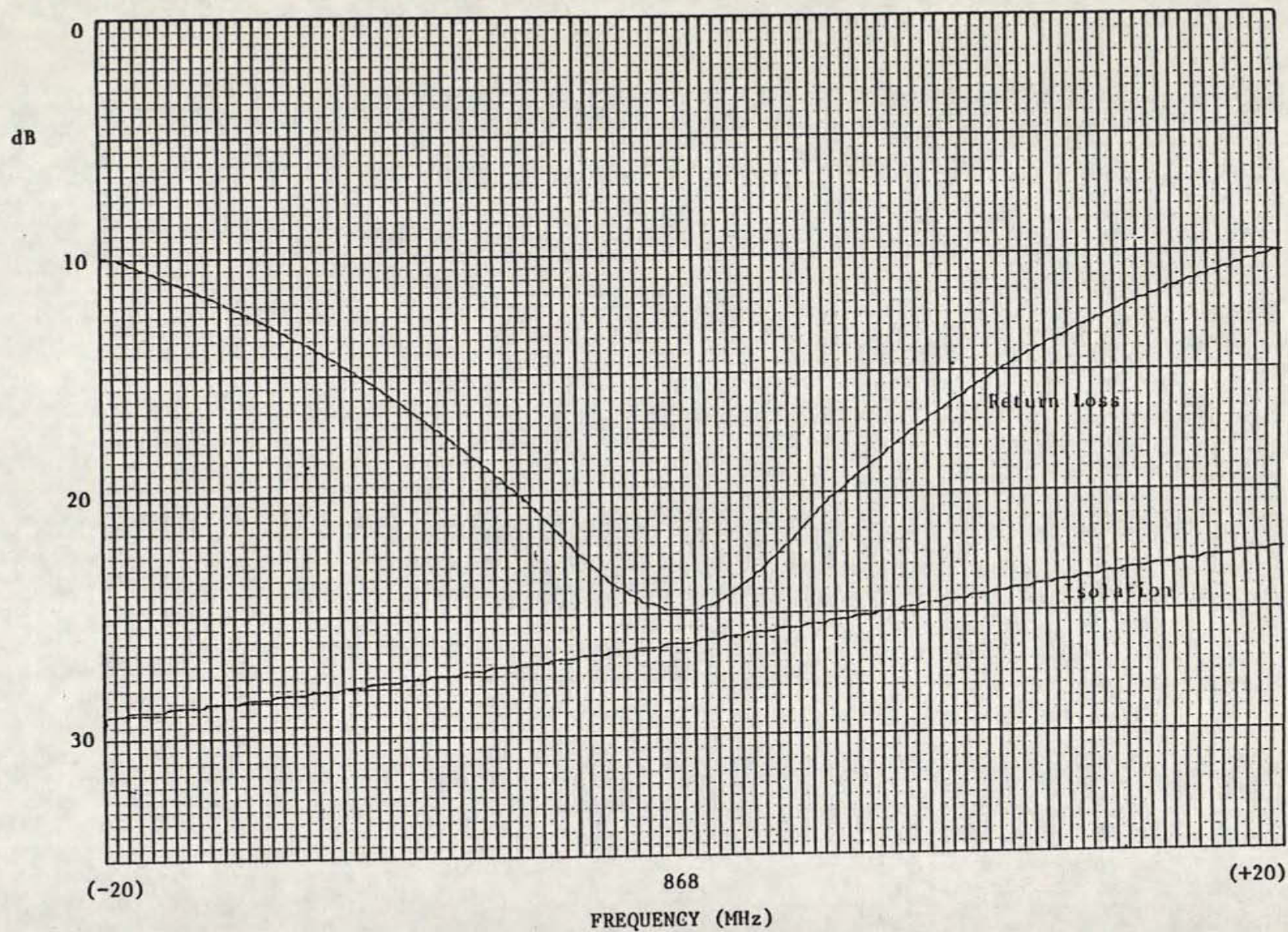


FIGURE 3.6 : MEASURED RETURN LOSS AND ISOLATION OF BREADBOARD TRANSMIT BAND ELEMENT (INPUT TO PORT 2)

DOCUMENT No.

REV.

TDE/MST/2500/001

SHEET



COM DEV



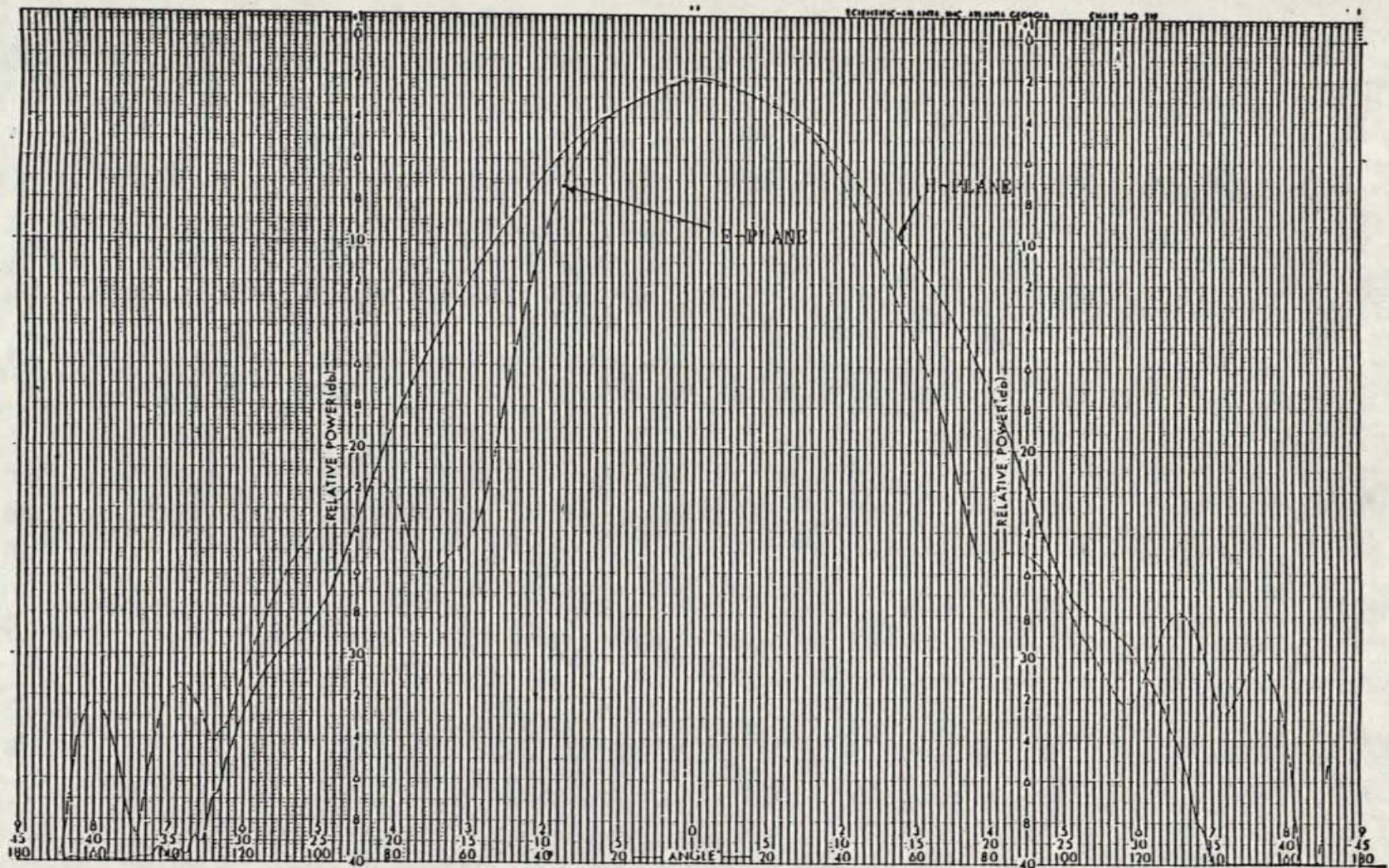


FIGURE 3.7 : MEASURED E- AND H-PLANE PATTERNS OF BREADBOARD RECEIVE BAND ELEMENT AT 823 MHz

DOCUMENT NO.

REV.

TDE/MST/2500/001



COM DEV

SHEET

28



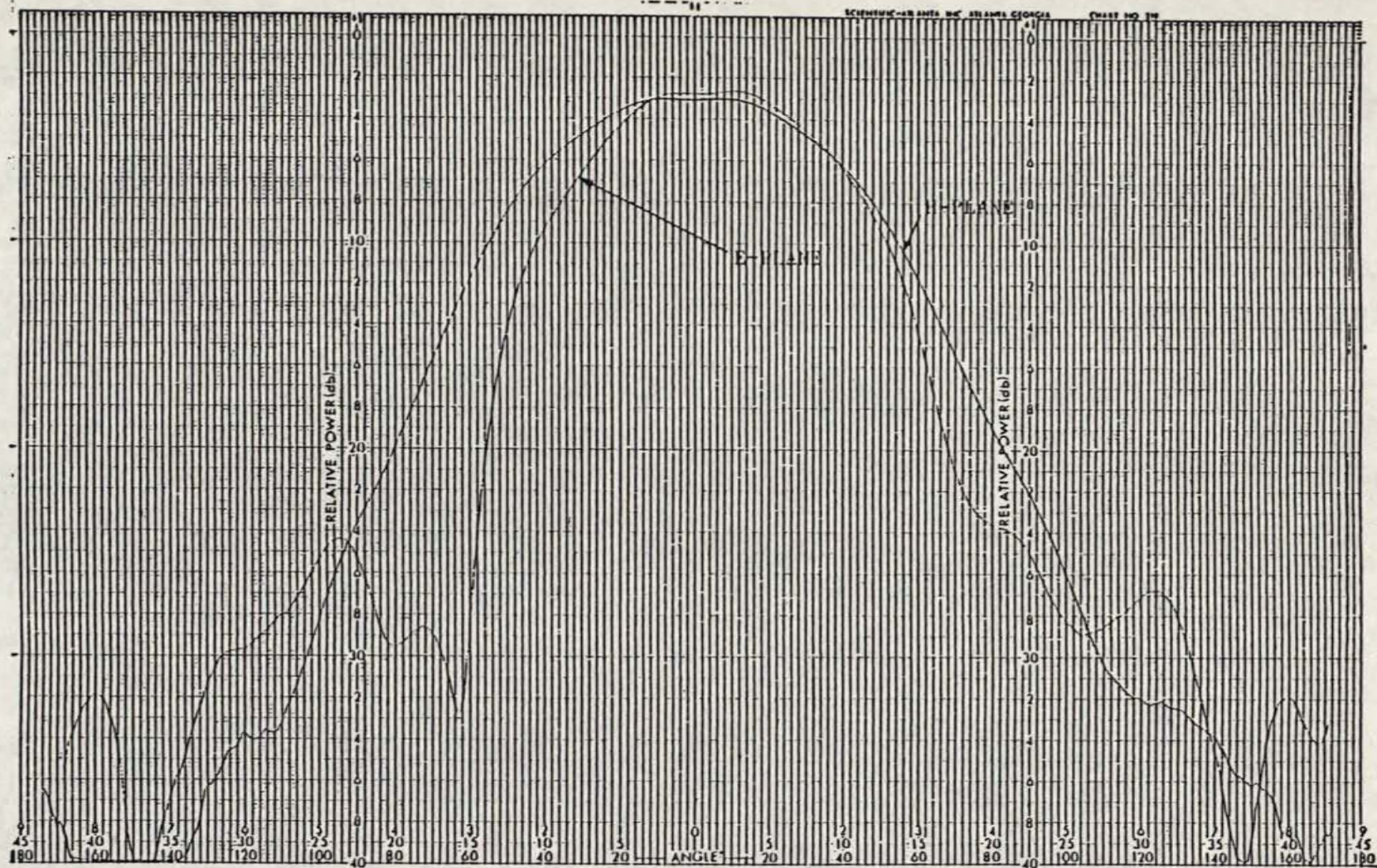


FIGURE 3.8 : MEASURED E- AND H-PLANE PATTERNS OF BREADBOARD TRANSMIT BAND ELEMENT AT 868 MHz

DOCUMENT NO.

REV.

TDE/MST/2500/001



COM DEV

SHEET

29

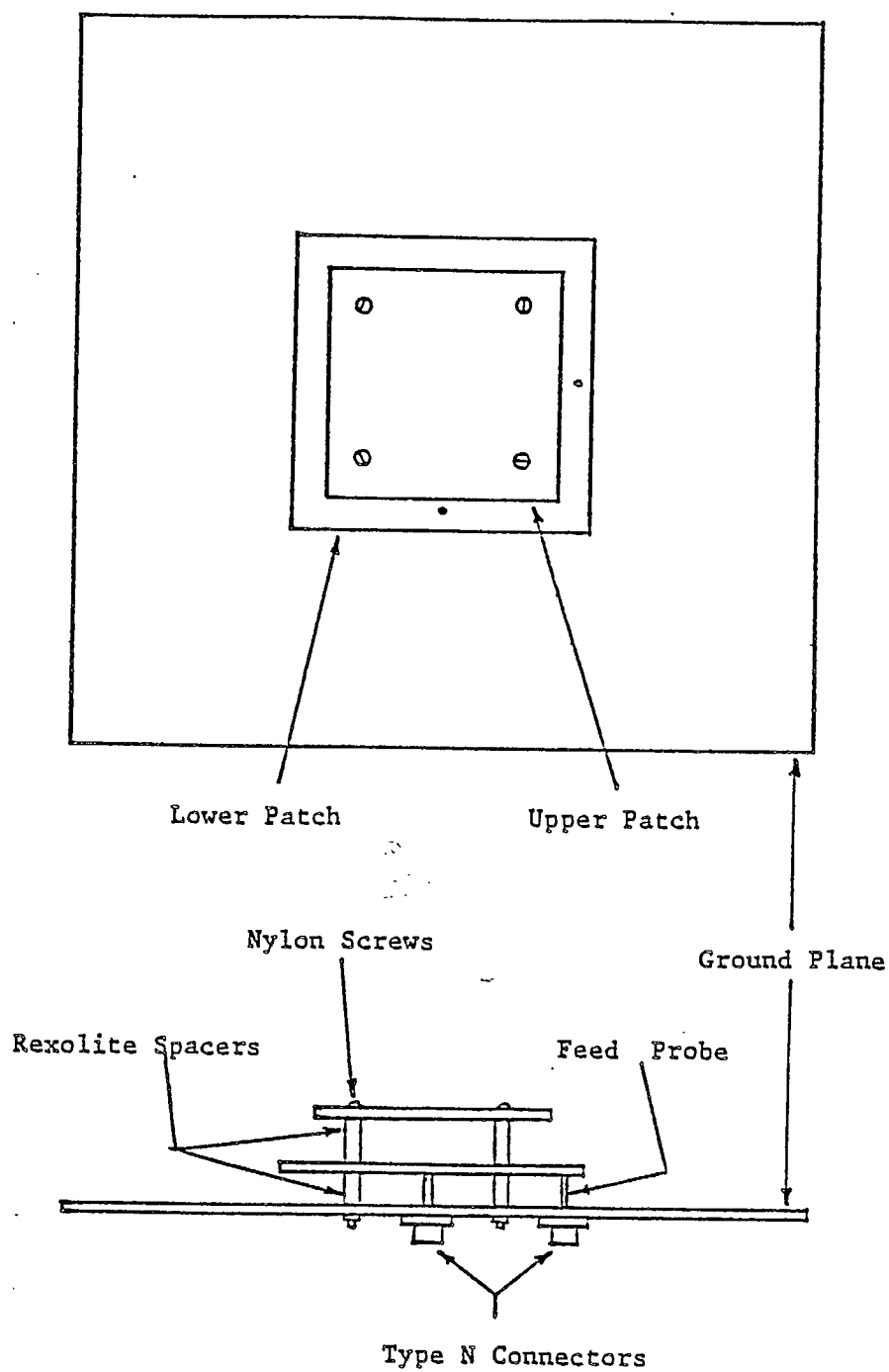


FIGURE 3.9: EXPERIMENTAL STACKED PATCH ANTENNA

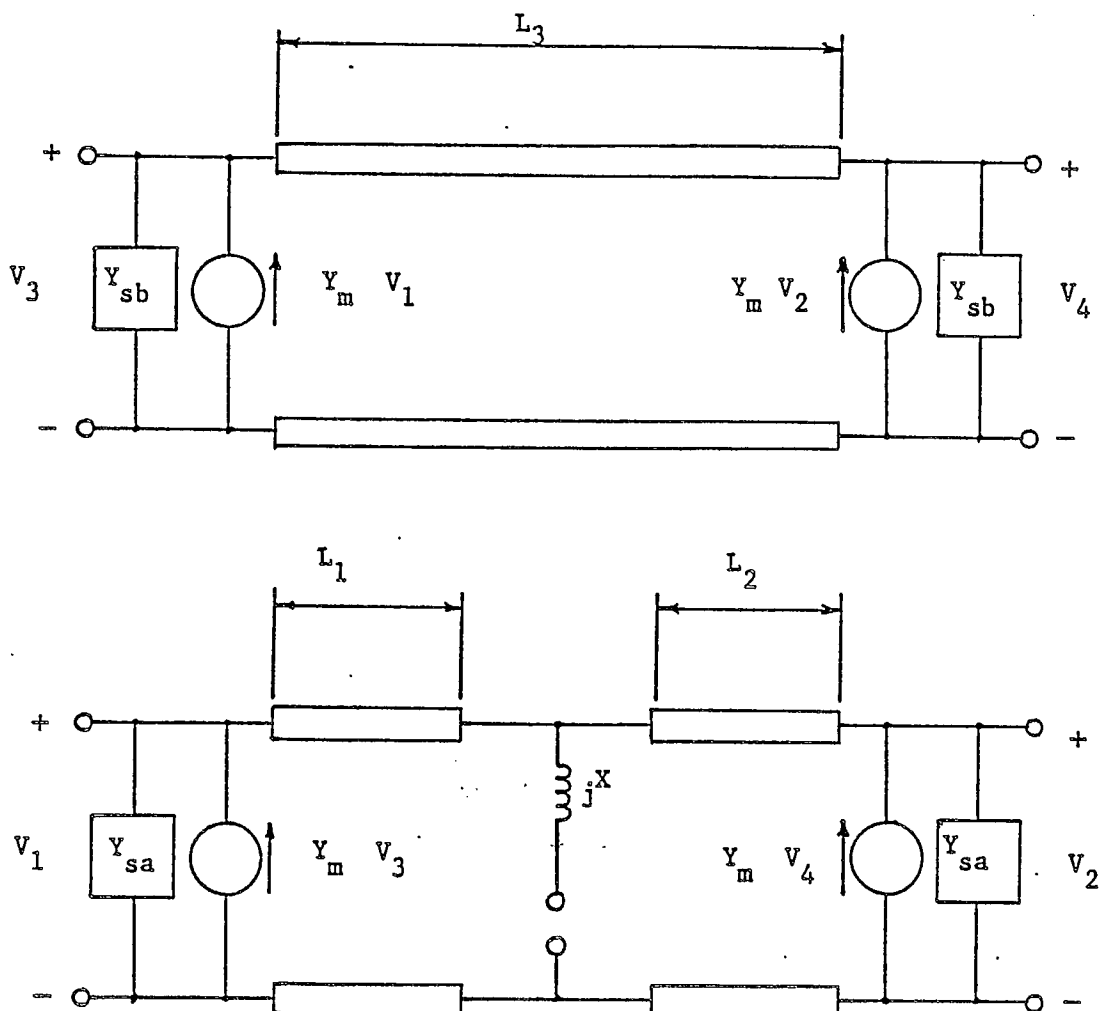


## 3.3.2

Characteristic of Stacked Air-Dielectric Square Patch Antenna

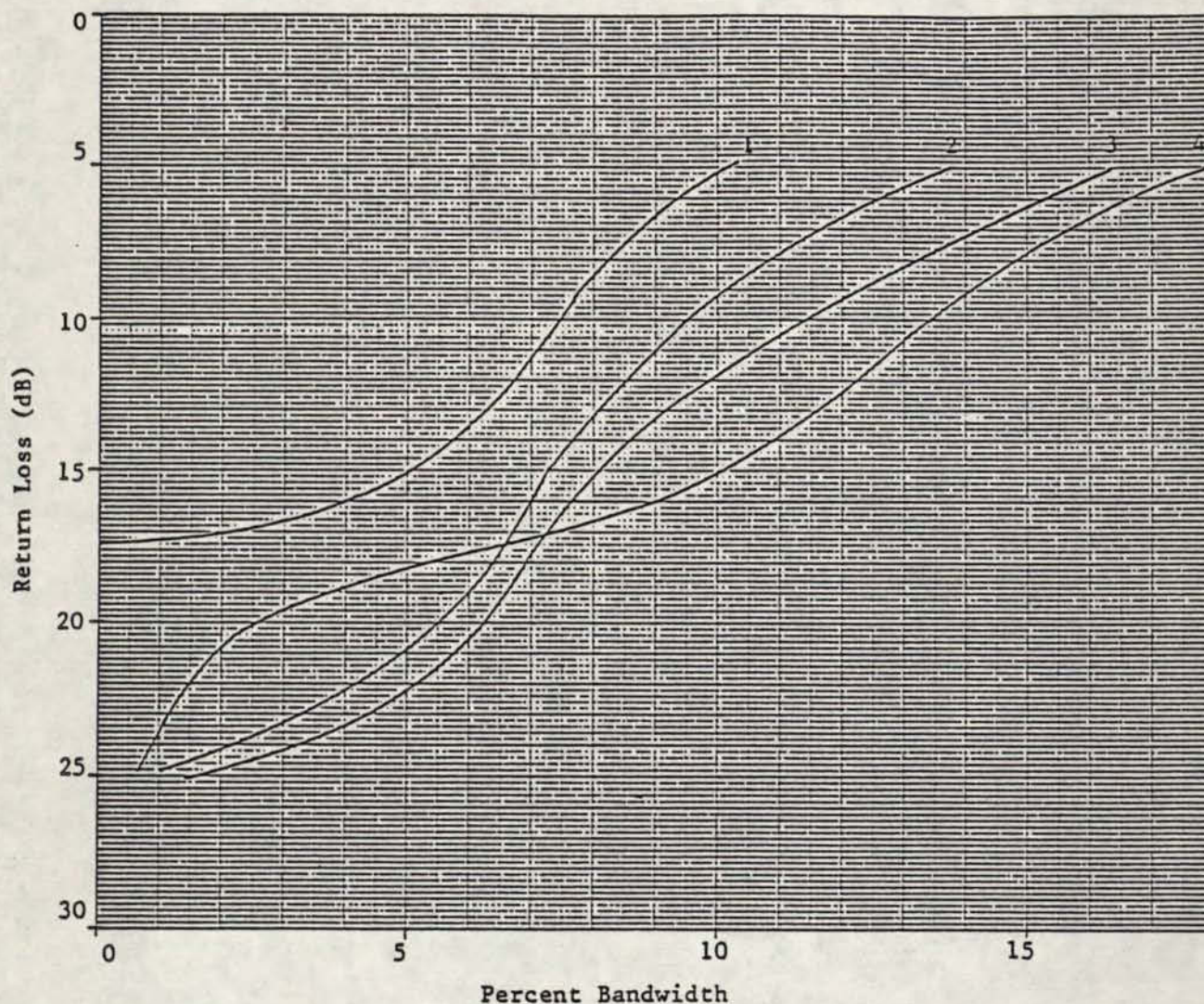
A transmission line model of the stacked patch geometry was developed. The equivalent circuit is shown in Figure 3.10. The lower patch and ground plane form one microstrip resonator, while the two patches form another. The two resonators are coupled by the fringing fields at the radiating edges. The radiation resistances, fringing field capacitances, microstrip line parameters and probe reactance are computed as for a single patch. Because of the way the upper cavity is modelled the case where the top patch is larger than the lower one is not correctly treated. In addition, a suitable expression for the mutual admittances was not found so the simplest approximation of the average of the two slot self-admittances, was used. Calculations using this model indicated that for best wideband performance the upper patch should be smaller than the lower one, the spacing between patches should be greater than between the lower patch and ground plane, and the feed probe should be connected to the lower ground plane near the edge. These trends were confirmed by experiment but the calculated input impedances were not very close to those measured. For this model to be truly useful substantial improvements are necessary. These were not pursued as empirical optimization was considered more effective.

An experimental parametric study was carried out in which the size of the upper square patch, the two spacings and the distance of the feed probe from the edge of the lower patch were variables. For each combination of patch sizes and spacings the probe was moved to the position giving the best return loss/bandwidth combination. In each case the frequency was swept from 700 MHz to 1100 MHz. Figure 3.11 shows the trade-off between return loss and bandwidth for several of the more successful combinations. At 20 dB return loss the maximum bandwidth achieved was 6.3 percent, exactly the requirement for



- $L_1$ : Lower Patch Length From Edge to Feed  
 $L_2$ : Lower Patch Length From Other Edge to Feed  
 $L_3$ : Upper Patch Length  
 $Y_m$ : Mutual Admittance Between Upper and Lower Slots  
 $Y_{sa}$ : Self Admittance of Lower Slots  
 $Y_{sb}$ : Self Admittance of Upper Slots  
 $jX$ : Feed Probe Reactance

FIGURE 3.10: EQUIVALENT CIRCUIT FOR STACKED PATCH ANTENNA



All cases: Lower patch 6.4 inches square, upper patch 5.5 inches square

- 1: Lower spacing 0.15 inch, upper spacing 0.45 inch
- 2: Lower spacing 0.25 inch, upper spacing 0.55 inch
- 3: Lower spacing 0.35 inch, upper spacing 0.55 inch
- 4: Lower spacing 0.45 inch, upper spacing 0.55 inch

FIGURE 3.11: RETURN LOSS AND BANDWIDTH OF STACKED PATCH ANTENNAS

MSAT. At a VSWR of 2 the best result was 13.8 percent bandwidth. The latter result was achieved with a total height above the ground plane of 1.12 inches or  $0.082 \lambda$  at the centre frequency of 860 MHz. Figure 3.12 shows a typical plot of return loss versus frequency. This shows clearly the dual resonance which gives rise to the wideband characteristic when the coupling between the two resonators is correct. Also shown on this plot is the isolation between two feed probes attached to adjacent sides of the lower patch as required for circular polarization using two feedpoints. If only the dominant resonant mode existed in each of the two cavities then there would be no coupling between the probes. The existence of such coupling demonstrates that higher order modes are excited at a low level.

Based on the data accumulated in the parametric study a bread-board antenna was designed for operation between 821 and 870 MHz. Figures 3.13 to 3.14 show the return loss and isolation measured at each input port. The element was centred in a 30 by 36 inch ground plane for these measurements. Clearly the scaling from a centre frequency of about 875 MHz (obtained in the parametric study) to 845 MHz has resulted in some deterioration of the performance. A summary of the return loss and isolation measurements is given in Table 3.3. The plots show that careful optimization could result in each required band falling in one of the dips in the return loss curve to obtain perhaps 23 dB worst case return loss levels, using the stacked patch geometry for a dual band response.



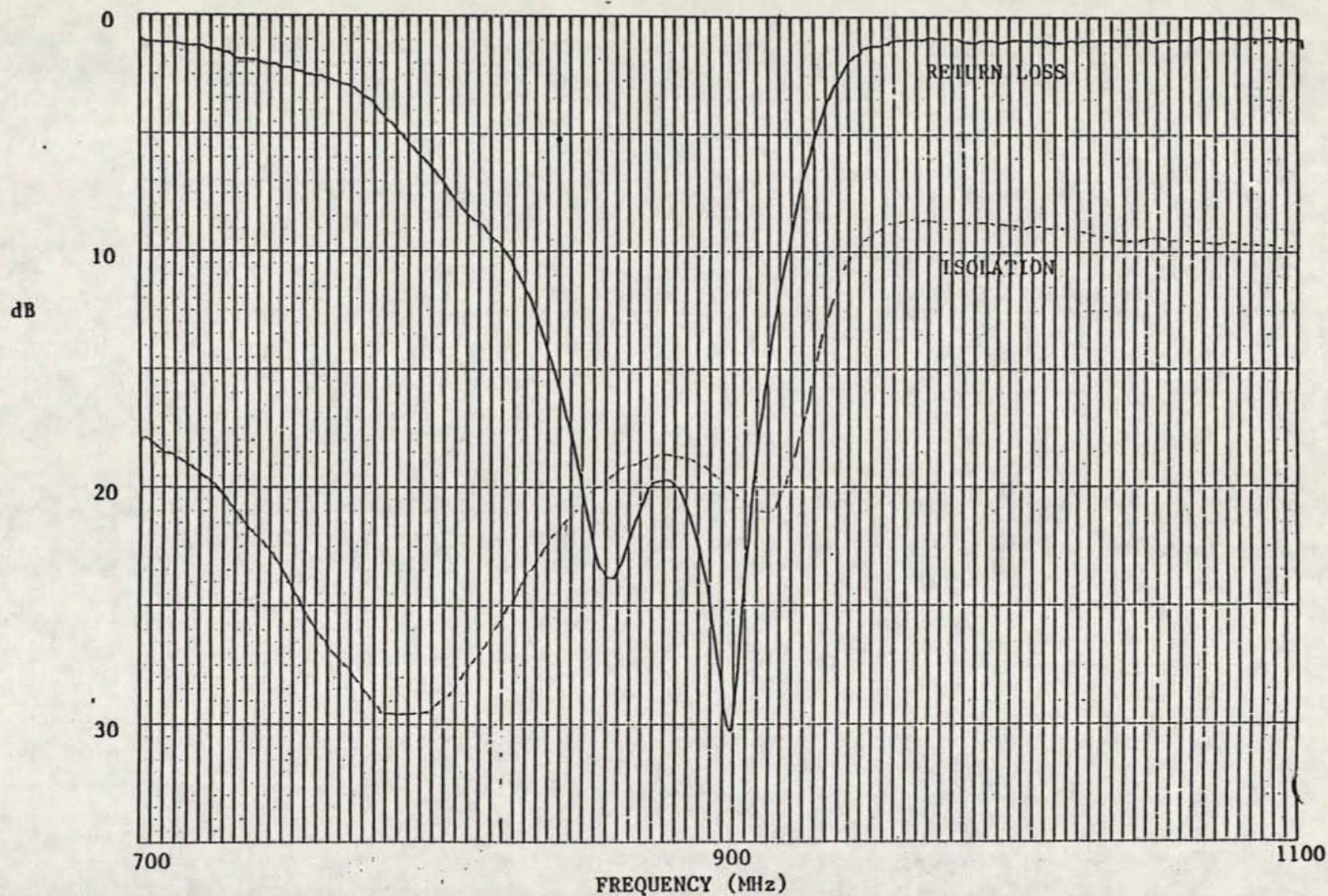


FIGURE 3.12: RETURN LOSS AND ISOLATION OF A STACKED AIR-DIELECTRIC SQUARE PATCH ANTENNA. LOWER PATCH 6.4 x 6.4 INCHES, SPACED 0.35 INCH FROM GROUND PLANE; UPPER PATCH 5.5 x 5.5 INCHES, SPACED 0.50 INCH FROM LOWER PATCH

DOCUMENT NO.

REV.

TDE/MST/2500/001

SHEET

35



COM DEV



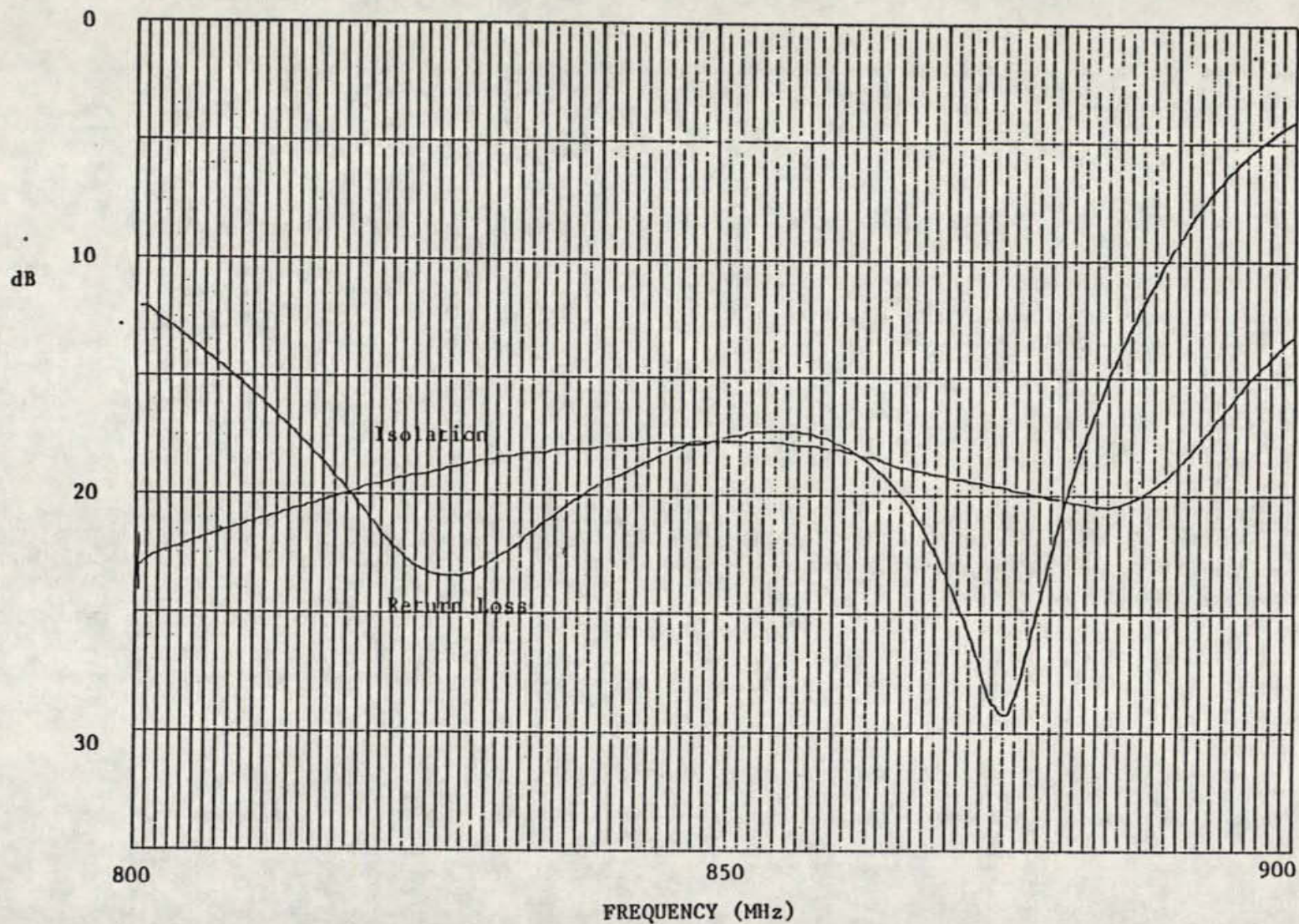


FIGURE 3.13: MEASURED RETURN LOSS AND PORT-TO-PORT ISOLATION OF BREADBOARD STACKED PATCH ANTENNA (INPUT TO PORT 1)

DOCUMENT NO.

TDE/MST/2500/001

REV.

—



COM DEV

SHEET

36



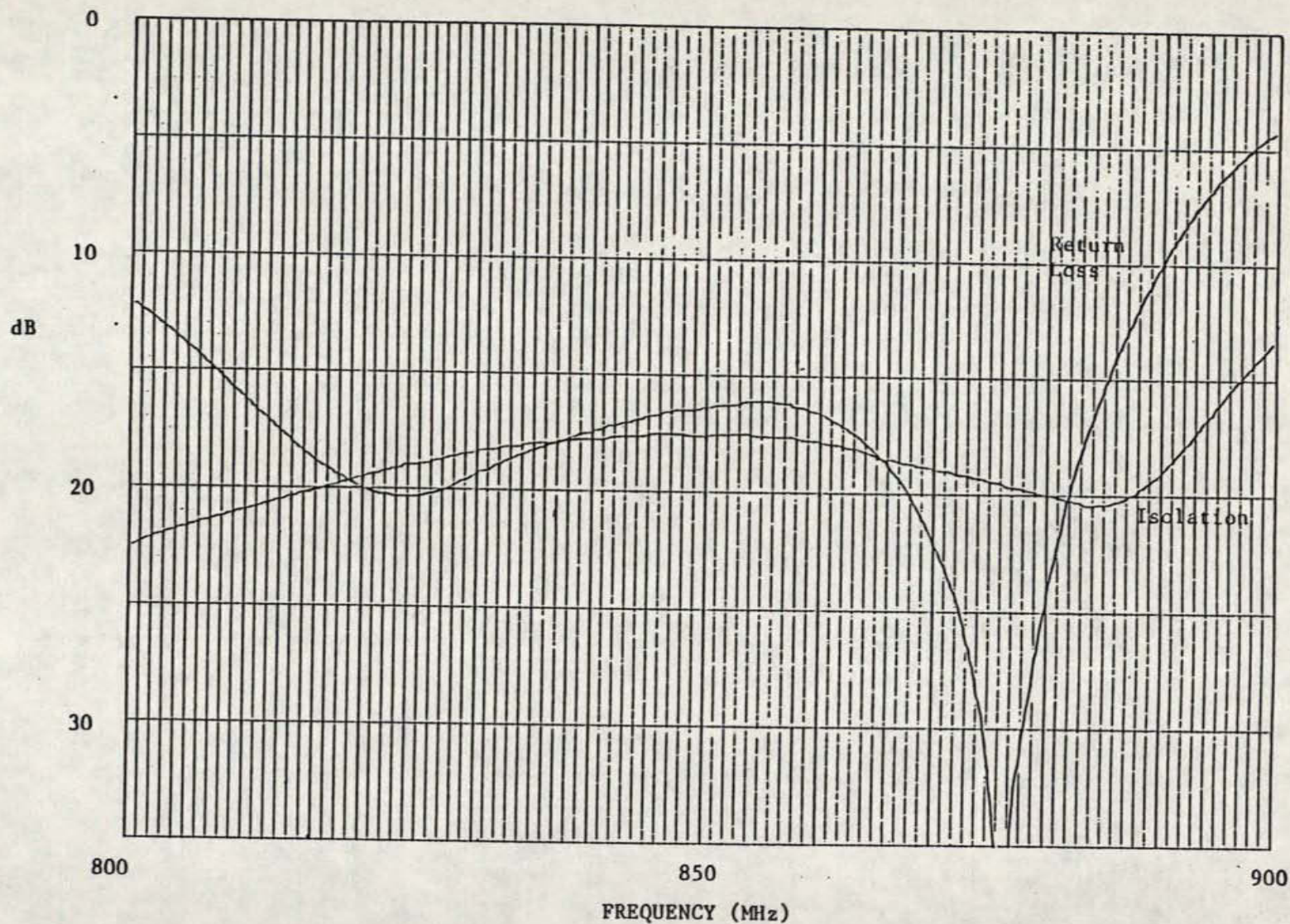


FIGURE 3.14: MEASURED RETURN LOSS AND PORT-TO-PORT ISOLATION OF BREADBOARD STACKED PATCH ANTENNA (INPUT TO PORT 2)

DOCUMENT NO.

REV.

TDE/MST/2500/001



COM DEV

SHEET

37



TABLE 3.3: RETURN LOSS AND ISOLATION SUMMARY  
FOR BREADBOARD STACKED PATCH ANTENNA

| <u>Frequency Band</u><br>(MHz) | <u>Return Loss (dB)</u> |               | <u>Isolation (dB)</u> |
|--------------------------------|-------------------------|---------------|-----------------------|
|                                | <u>Port 1</u>           | <u>Port 2</u> |                       |
| 821 - 825                      | 21.6                    | 20.1          | 19.0                  |
| 866 - 870                      | 20.0                    | 18.7          | 18.5                  |
| 821 - 870                      | 17.3                    | 16.1          | 17.7                  |
| with thermal allowance         |                         |               |                       |
| 819 - 827                      | 20.4                    | 19.6          | 18.8                  |
| 864 - 872                      | 19.0                    | 17.8          | 18.4                  |
| 819 - 872                      | 17.3                    | 16.1          | 17.7                  |

The radiation patterns of this breadboard element have been measured at 823 MHz and 868 MHz. These are plotted in Figures 3.15 and 3.16 respectively. Again some effects of the finite ground plane are seen on the patterns near boresight. The beamwidths and squints are summarized in Table 3.4.

### 3.3.3 Mutual Coupling Between Stacked Patch Antennas

Published data regarding mutual coupling between wideband or dual band stacked patch antennas is scarce. Using two of the breadboard air-dielectric stacked square patch antennas, mounted on the 30 by 36 inch ground plane a number of mutual coupling measurements were carried out. Measurements of E- and H-plane coupling were made as shown in Figure 3.17, with the unused feed ports terminated. There was no observable difference in coupling with the unused ports open circuited. The measurements were made as a function of frequency between 810 MHz and 880 MHz at several spacings between the elements. The coupling changed slowly with frequency, being slightly stronger at the lower end of the frequency range. There was no evidence of the antenna resonances in the mutual coupling data. In Figure 3.18 are shown the values of E- and H- plane coupling at 820 MHz plotted against the element spacing. Figure 3.19 contains the corresponding curves for 870 MHz. The magnitude of the coupling is similar to that existing between single patches and to that given in the literature for stacked patches. At the 12 inch spacings suggested in Section 2 the coupling values at 820 MHz are -23 dB (E-plane) and -27 dB (H-Plane) and at 870 MHz they are -26 dB (E-plane) and -28 dB (H-plane).

Another set of measurements were performed with two breadboard stacked patch elements positioned to correspond to locations in a 12 inch spaced triangular grid as could be used in a septet-based feed array. Three geometries were used which cover all the

Her Majesty the Queen in Right of Canada (1986) as represented by the Minister of Supply And Services.

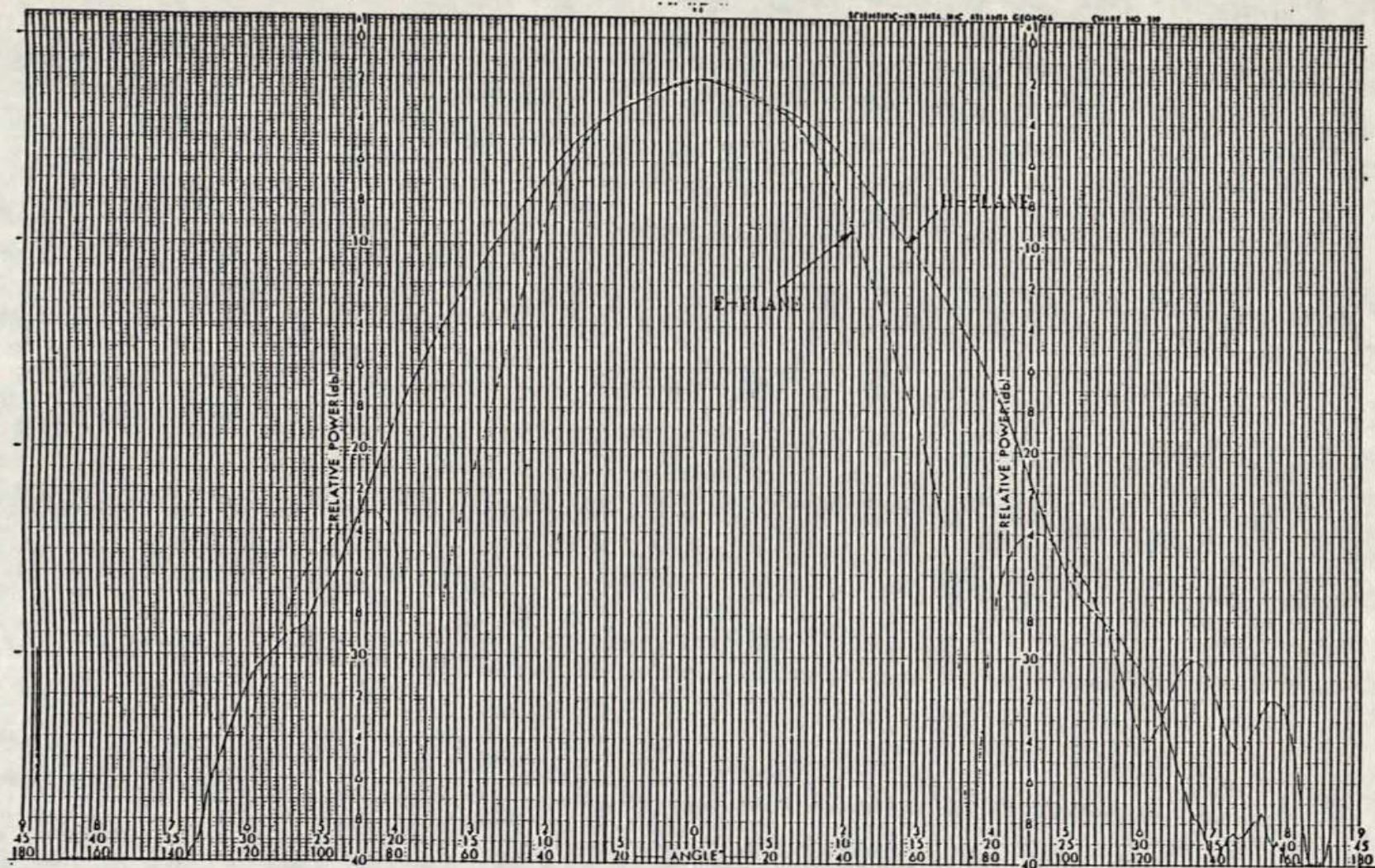


FIGURE 3.15: MEASURED E- AND H-PLANE PATTERNS OF BREADBOARD STACKED PATCH ELEMENT AT 823 MHz


DOCUMENT No.

REV.

TDE/MST/2500/001

SHEET

40


**COM DEV**



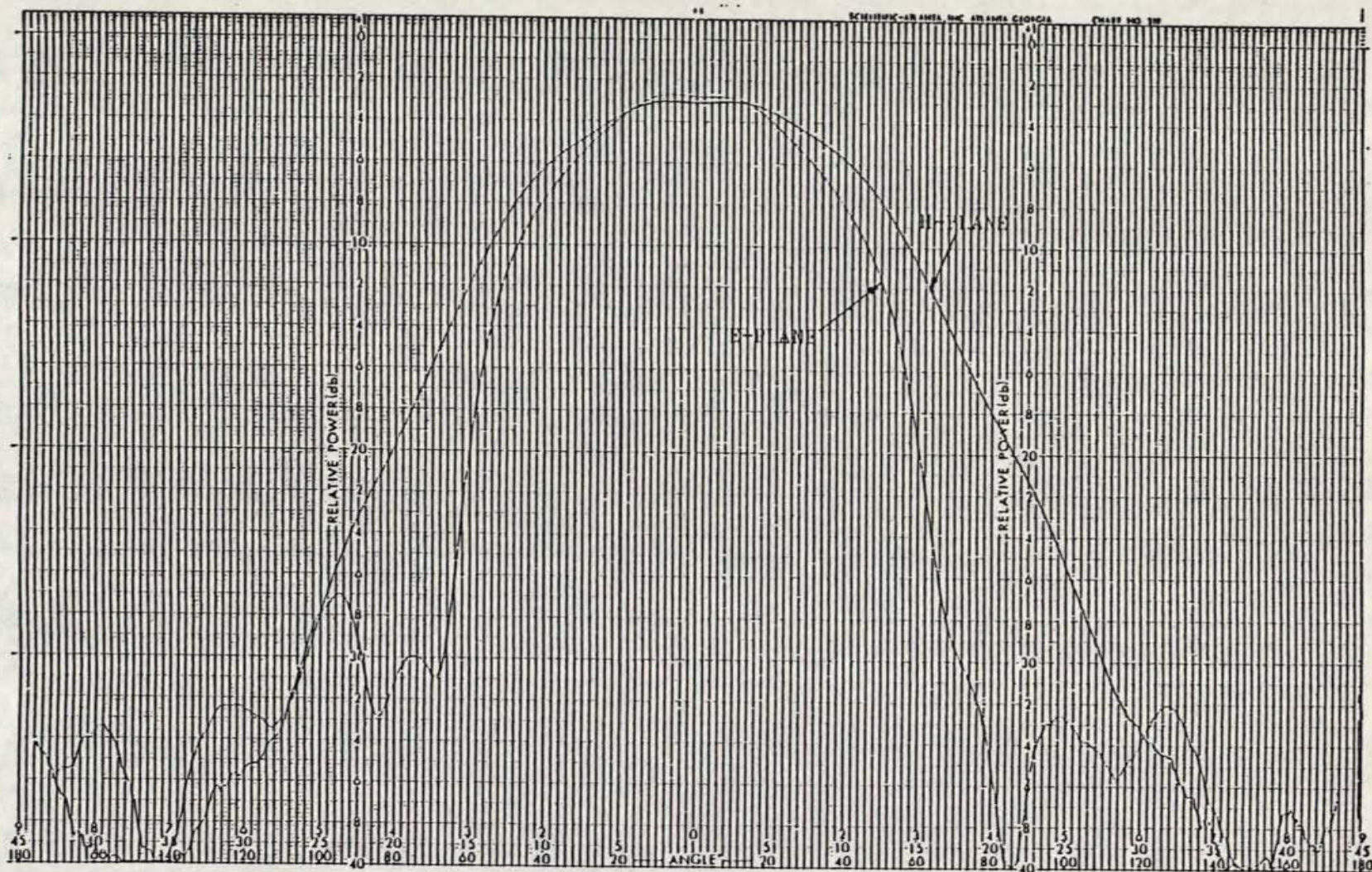


FIGURE 3.16: MEASURED E- AND H-PLANE PATTERNS OF BREADBOARD STACKED PATCH ELEMENT AT 868 MHz

DOCUMENT No.

REV.

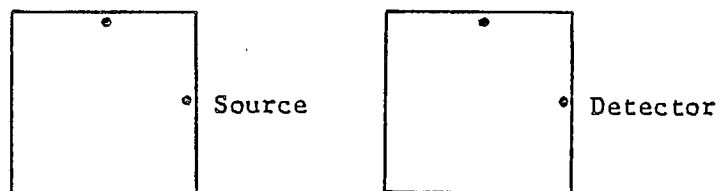
TDE/MST/2500/001

**COM DEV**

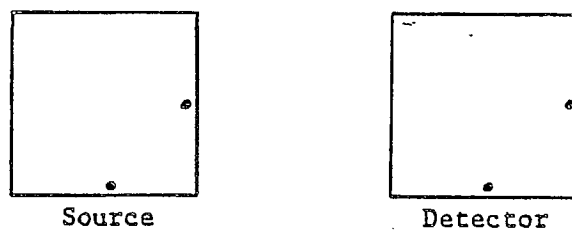
SHEET 41

TABLE 3.4: BEAMWIDTHS AND SQUINT OF BREADBOARD  
STACKED PATCH ELEMENT

|         | Half-Power Beamwidth<br><u>(degrees)</u> | Squint<br><u>(degrees)</u> |
|---------|--|----------------------------|
| 823 MHz |  |                            |
| E-plane | 61                                       | 0.5                        |
| H-plane | 68                                       | 2.0                        |
| 868 MHz |  |                            |
| E-plane | 61                                       | 0.5                        |
| H-plane | 79                                       | 1.5                        |



E-Plane Coupling



H-Plane Coupling

FIGURE 3.17: GEOMETRY OF E- and H-PLANE MUTUAL COUPLING

COM DEV LTD

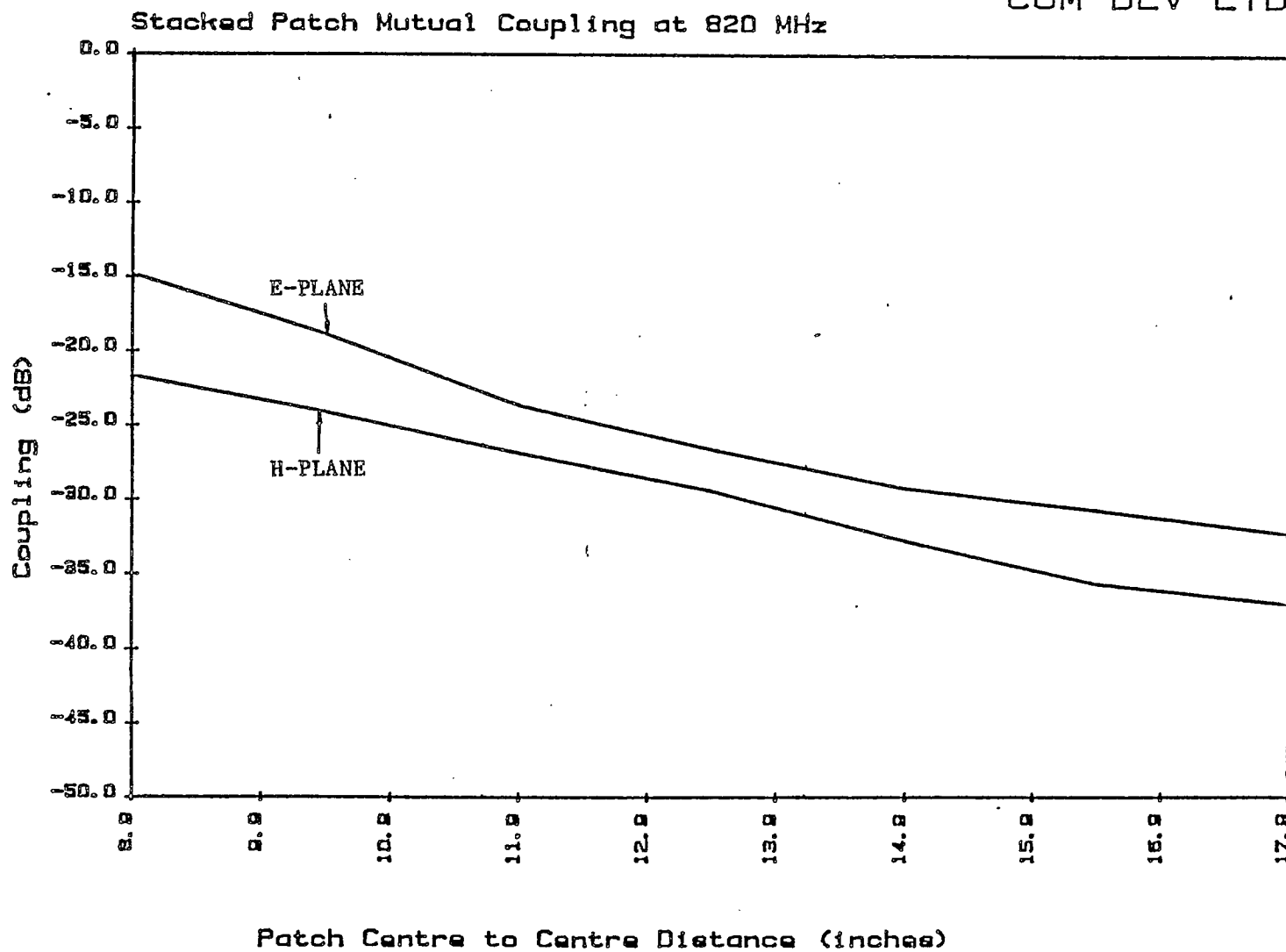


FIGURE 3.18: MEASURED E- AND H-PLANE MUTUAL COUPLING VERSUS SPACING BETWEEN BREADBOARD STACKED PATCH ANTENNAS AT 820 MHz

COM DEV LTD

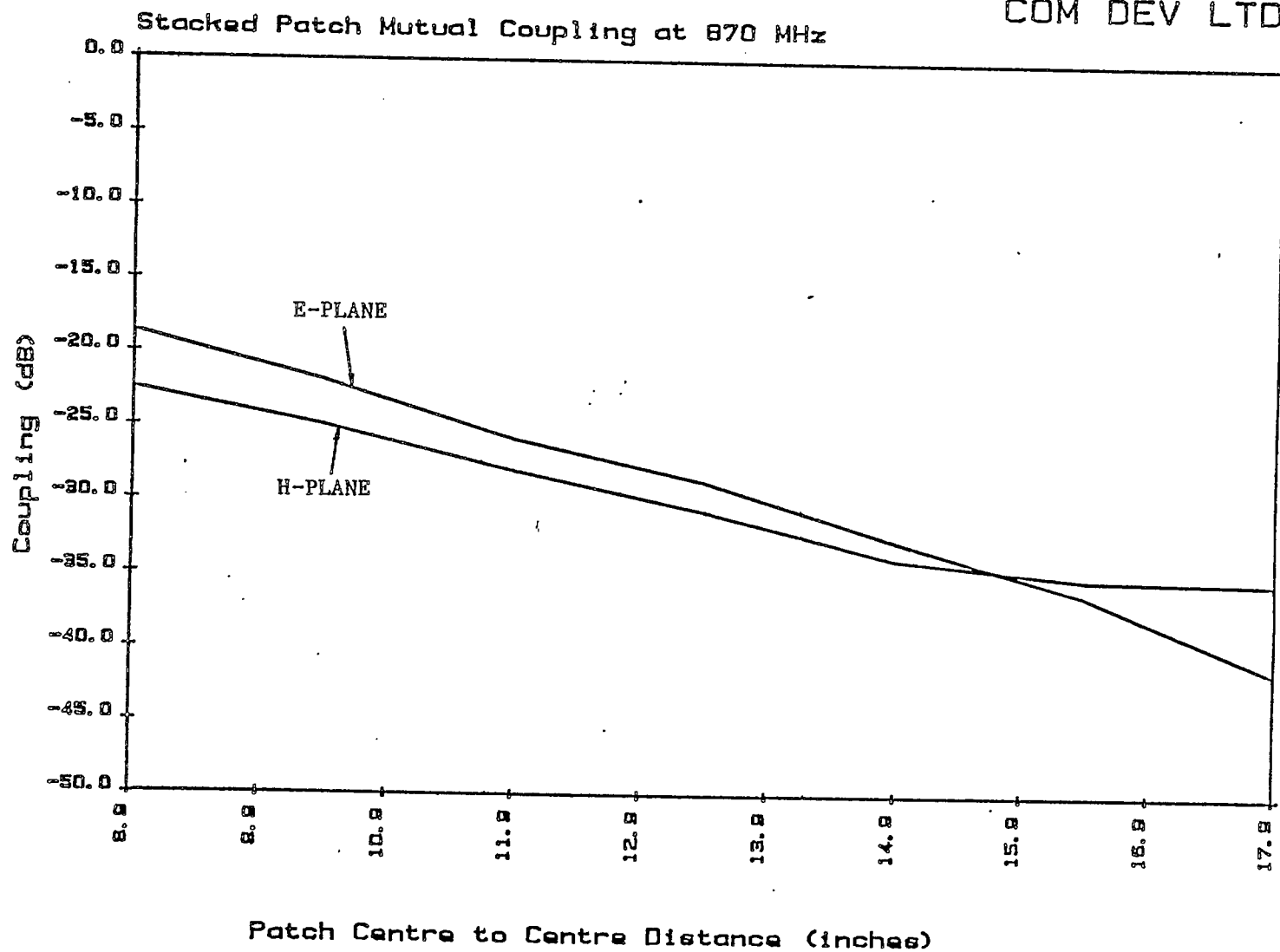
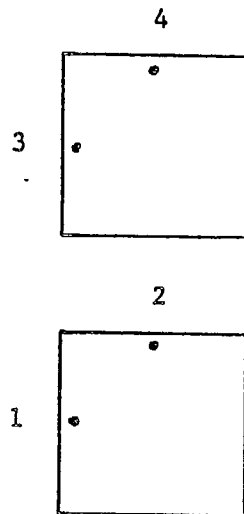
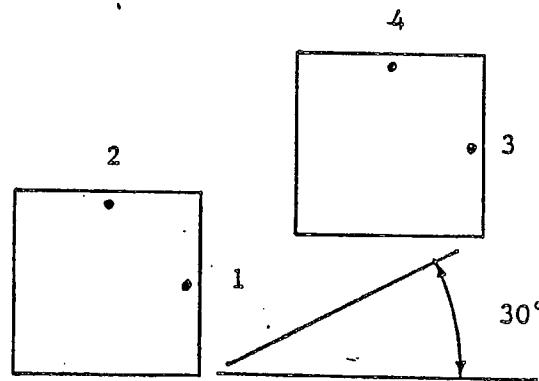


FIGURE 3.19: MEASURED E- AND H-PLANE MUTUAL COUPLING VERSUS SPACING BETWEEN BREADBOARD STACKED PATCH ANTENNAS AT 870 MHz

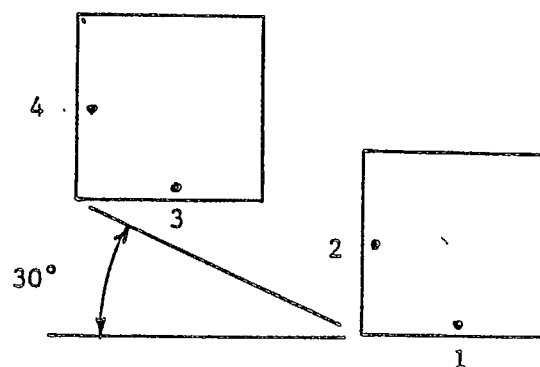




Case 1



Case 2



Case 3

FIGURE 3.20: SEPTIET COUPLING GEOMETRIES (VIEWED TOWARD FRONT FACE, ALL CASES 12 IN. CENTRE-TO-CENTRE SPACING)


TABLE 3.5: MUTUAL COUPLING BETWEEN STACKED PATCH ANTENNAS IN SEPTET CONFIGURATIONS

| Frequency<br>(MHz) | $S_{13}$     |                 | $S_{14}$     |                 | $S_{23}$     |                 | $S_{24}$     |                 |
|--------------------|--------------|-----------------|--------------|-----------------|--------------|-----------------|--------------|-----------------|
|                    | Loss<br>(dB) | Angle<br>(deg.) | Loss<br>(dB) | Angle<br>(deg.) | Loss<br>(dB) | Angle<br>(deg.) | Loss<br>(dB) | Angle<br>(deg.) |
| Case 1             |              |                 |              |                 |              |                 |              |                 |
| 820                | 27.2         | -45.5           | 36.7         | 45.4            | 36.6         | 159.9           | 23.6         | 30.3            |
| 825                | 27.4         | -60.7           | 36.3         | 38.1            | 36.5         | 154.9           | 24.0         | 23.8            |
| 865                | 29.0         | -165.4          | 36.7         | -30.4           | 42.6         | 92.8            | 25.8         | -65.2           |
| 870                | 28.0         | 175.7           | 36.7         | -42.0           | 48.1         | 74.7            | 25.9         | -91.8           |
| Case 2             |              |                 |              |                 |              |                 |              |                 |
| 820                | 27.3         | 35.8            | 25.8         | 83.3            | 25.6         | 72.6            | 34.2         | -31.4           |
| 825                | 28.1         | 29.9            | 26.1         | 73.1            | 25.8         | 62.4            | 39.1         | -41.4           |
| 865                | 30.9         | -62.5           | 28.7         | -17.5           | 27.6         | -23.4           | 39.9         | -144.8          |
| 870                | 31.9         | -99.5           | 29.1         | -36.3           | 28.2         | -40.8           | 33.7         | -170.5          |
| Case 3             |              |                 |              |                 |              |                 |              |                 |
| 820                | 28.7         | -28.6           | 30.7         | -95.6           | 26.7         | -127.3          | 25.0         | 19.6            |
| 825                | 30.7         | -36.2           | 30.6         | -104.8          | 26.4         | -136.2          | 25.7         | 10.5            |
| 865                | 31.8         | -134.1          | 33.8         | 159.9           | 28.4         | 145.4           | 28.1         | -84.6           |
| 870                | 29.7         | -160.4          | 35.2         | 141.7           | 29.5         | 132.7           | 28.6         | -114.2          |

DOCUMENT NO.

TDE/MST/2500/001

REV.


  
SHEET 47

couplings between adjacent patches in such an array with all the feeds aligned in the same direction. These geometries are shown in Figure 3.20. The measured couplings are tabulated in Table 3.5 for the frequencies 820, 825, 865 and 870 MHz.

These mutual coupling measurements include only the port characteristics of the elements. It is possible that modes may be generated by mutual coupling which are not detected at the feedpoints. These may, nevertheless, have an effect on the radiation patterns. It will be necessary to conduct measurements of the patterns of elements in an array to determine if any significant phenomena occur.

#### 3.4 Power Handling Capability of Patch Elements

The power level at which the single or stacked patch elements can safely operate is potentially limited by the temperature rise due to power dissipation, passive intermodulation and multipactor discharge. With suitable choice of materials and proper attention to making a good connection between the patch and feed probes there should be no difficulty with PIM in the antenna element itself. The beam forming network will probably be the worst area for PIM.

The power dissipation ability of the patches is severely limited by the minimal thermal contact between the layers. In addition the actual loss of the elements is not known although at least in the case of the single patch it is reasonable to assume less than 0.1 dB loss, corresponding to 1.4 W dissipation for 60 W input. The stacked patch will probably have greater loss than the single patch because of the two resonators. Development of a good theoretical model of the stacked patch element would lead to a prediction of loss. The loss values are too small to be conveniently determined by gain measurement. Alternatively the temperature rise could be measured with high RF power applied,

preferably under vacuum. While currently difficult to quantify, it is not expected that power dissipation will be a major problem.

Multipactor discharge is another condition which is very difficult to test for in an antenna. As it only occurs under vacuum, the tests must be held in a vacuum anechoic environment. Potentially a breakdown could occur between the lower patch and ground plane of the stacked patch antenna. The maximum voltage occurs near the feed point which is matched to 50 ohms so it may be assumed that the power at which breakdown occurs corresponds to the expected breakdown voltage of at least 250 V for a 0.35 inch gap between parallel plates at 868 MHz, corresponding to a power of 1.25 kW, which should be sufficient. Therefore it would probably be useful to attempt a measurement. The single patch with a wider 0.50 inch spacing should require about twice the power to produce multipaction, compared to the stacked patch. If, instead of using a small number of dielectric posts, the patch was supported on a continuous layer of material such as shuttle tile, having a low dielectric constant but very small voids, the danger of multipactor breakdown could probably be eliminated completely.

#### 4.0 BEAM FORMING NETWORK TECHNOLOGY

##### 4.1 Transmission Line Options

Each beam forming network required for MSAT will consist of a multi-way power divider network with unequal output powers and well controlled phases. It will be made up of a number of two-output power dividers interconnected with transmission lines (including bends and possibly fixed phase shifters and connections between layers of a multilayer structure). The two-way power dividers will probably be in the form of directional couplers with good isolation between the output ports in order to minimize effects due to reflections and mutual coupling of the array elements.

In the feed array panel envisaged in this report each patch element is fed by two probes passing through the ground plane from a stripline coupler underneath it which is in turn fed by a beam-forming network occupying one or more layers underneath for suppression of the parallel plate waveguide mode. Suitable prevention methods may include smearing of bolted joints with conductive adhesive (which may suffer from problems at low temperatures) or use of fastening techniques such as dip-brazing. With due care any excessive PIM levels can be eliminated.



#### 4.2 Experimental Coupler Design

As part of the investigation of technology suitable for the MSAT beam-forming network a stripline branch-line coupler was developed. For compactness a two-branch design was adopted, using as a baseline air-spaced stripline. Suppression of the parallel-plate waveguide mode (using several pins around connector probes) and matching using stripline extensions beyond the connector probes were found to be necessary for acceptable performance to be achieved.

The measured performance of this coupler is shown in Figure 4.1 (Return Loss), 4.2 (Isolation), 4.3 (Straight-through Loss) and 4.4 (Coupled Port Loss).

This value of overall loss is plotted in Figure 4.5. A smoothed curve is in good agreement with predictions of about 0.09 dB loss. As expected for this type of coupler the phase difference is almost exactly 90 degrees over the useful bandwidth of the device.

An ideal coupler of this type has return loss and isolation curves that track exactly and reach a value of 19 dB at six percent above the centre frequency. For a centre frequency of 845 MHz this corresponds to about 896 MHz. The measured return loss of 17.8 dB and isolation of 18.9 dB at 895 MHz demonstrate that the experimental coupler closely approaches the theoretical limit.

#### 4.3 Recommendations for BFN Development

This preliminary work on stripline with largely air/vacuum dielectric has demonstrated that it should be considered a viable medium for UHF spacecraft beam formers. However, there are a number of clear limitations which will have to be taken into account in the design of an actual BFN and feed array.





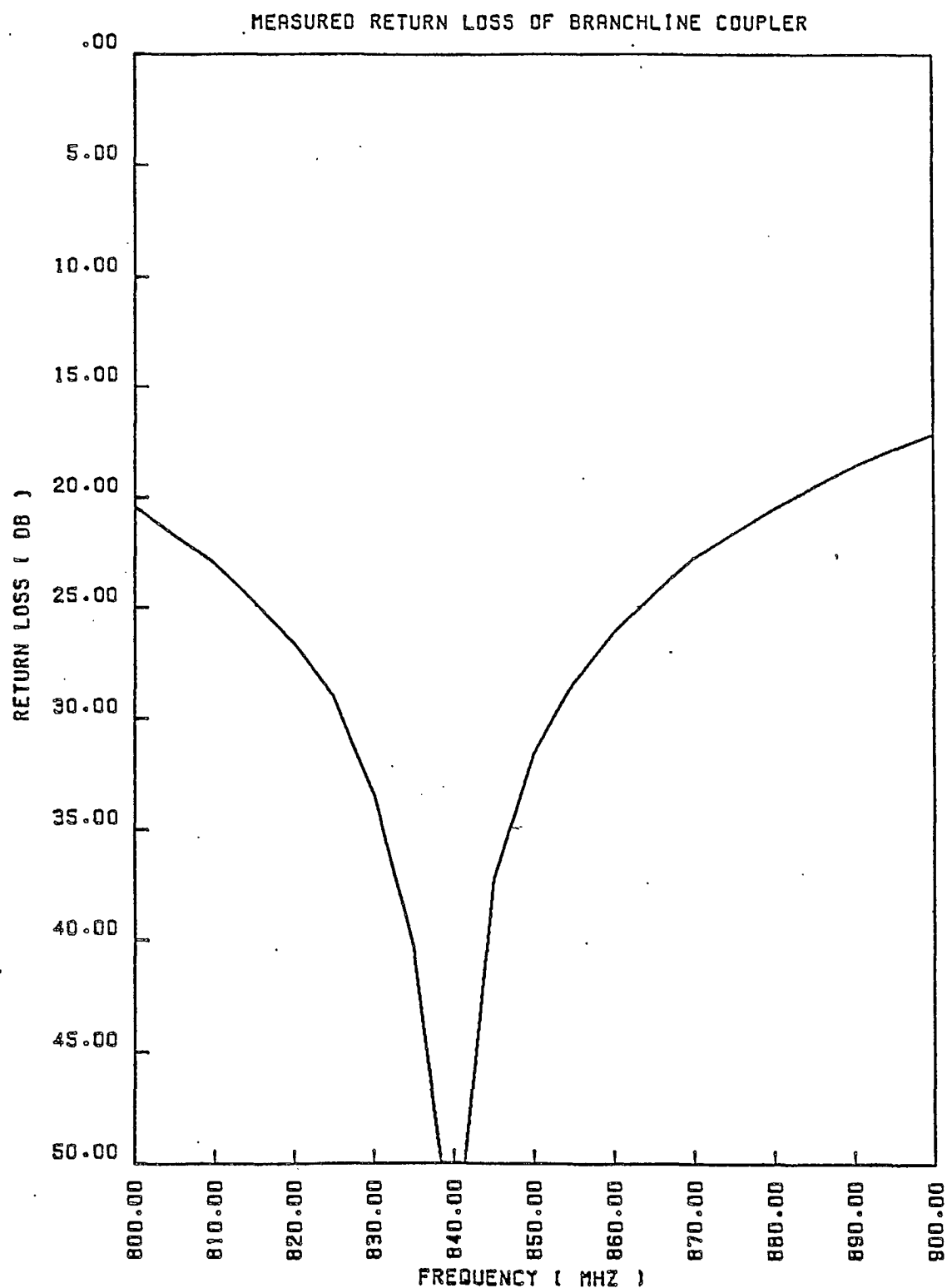


FIGURE 4.1: MEASURED RETURN LOSS OF STRIPLINE COUPLER

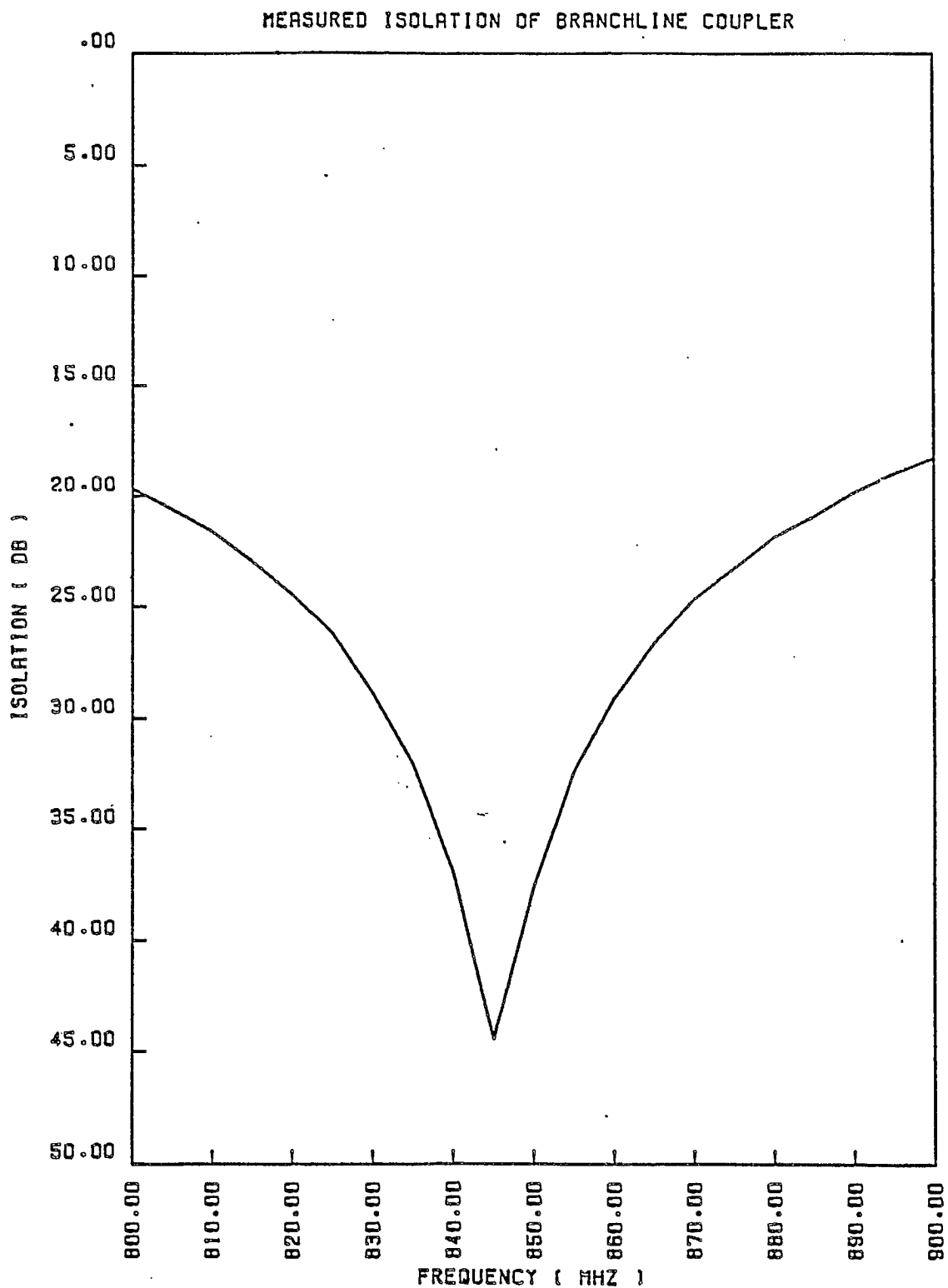


FIGURE 4.2: MEASURED ISOLATION OF STRIPLINE COUPLER

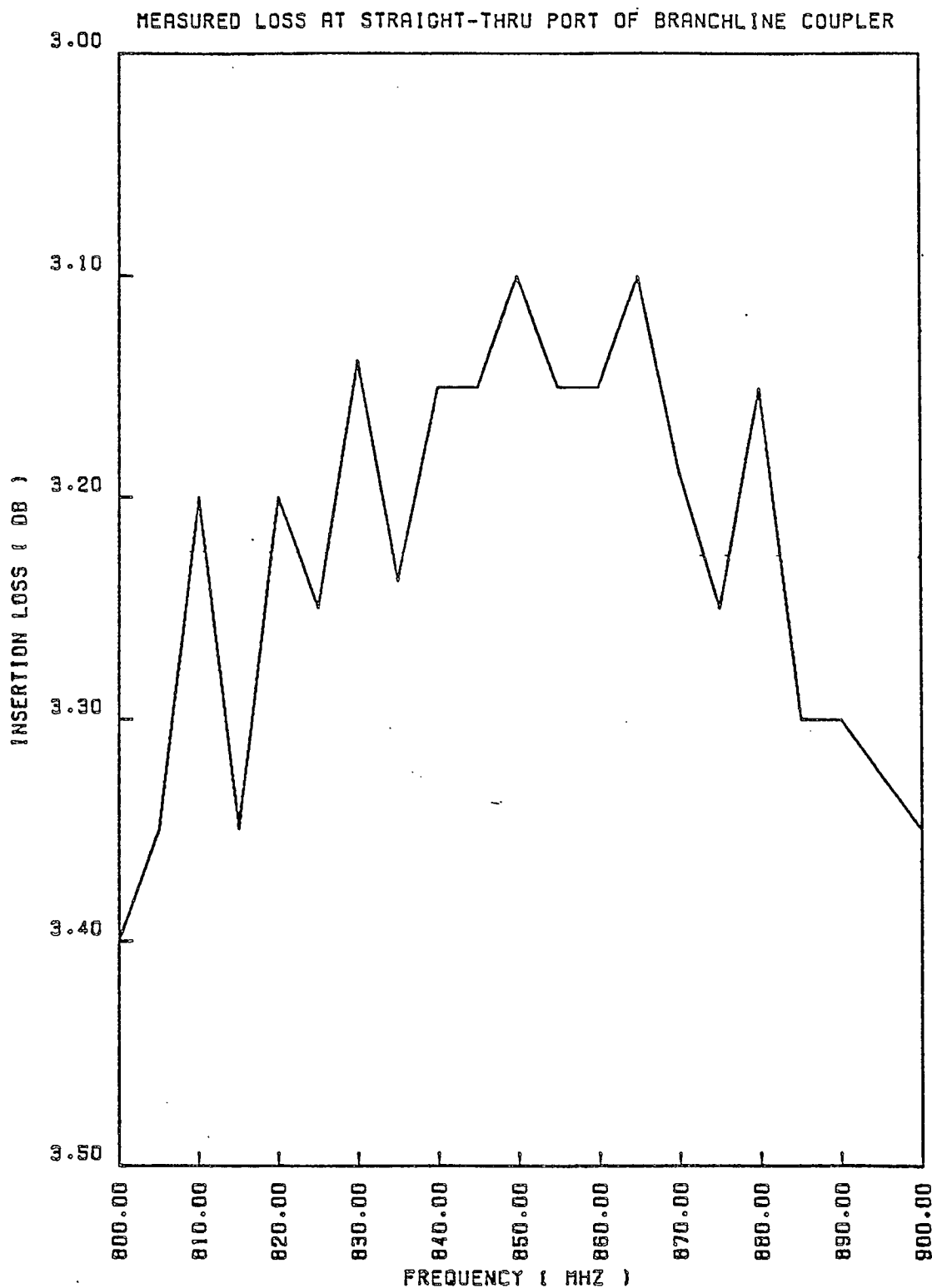


FIGURE 4.3: MEASURED STRAIGHT-THROUGH LOSS OF STRIPLINE COUPLER

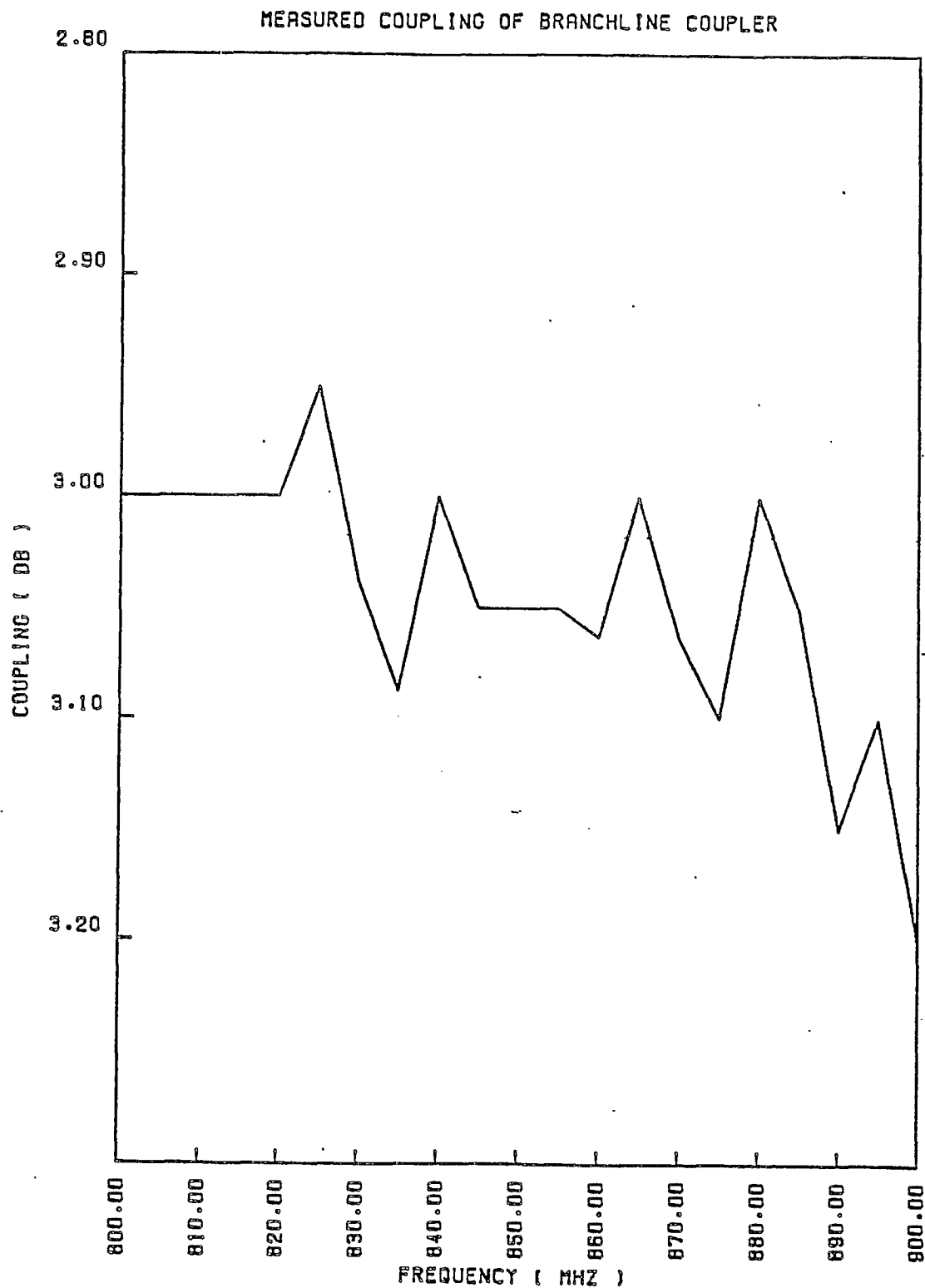



FIGURE 4.4: MEASURED COUPLING OF STRIPLINE COUPLER

|                  |      |  |
|------------------|------|--|
| DOCUMENT No.     | REV. |  <b>COM DEV</b> |
| TDE/MST/2500/001 | —    |  |
|                  |      | SHEET 55   |



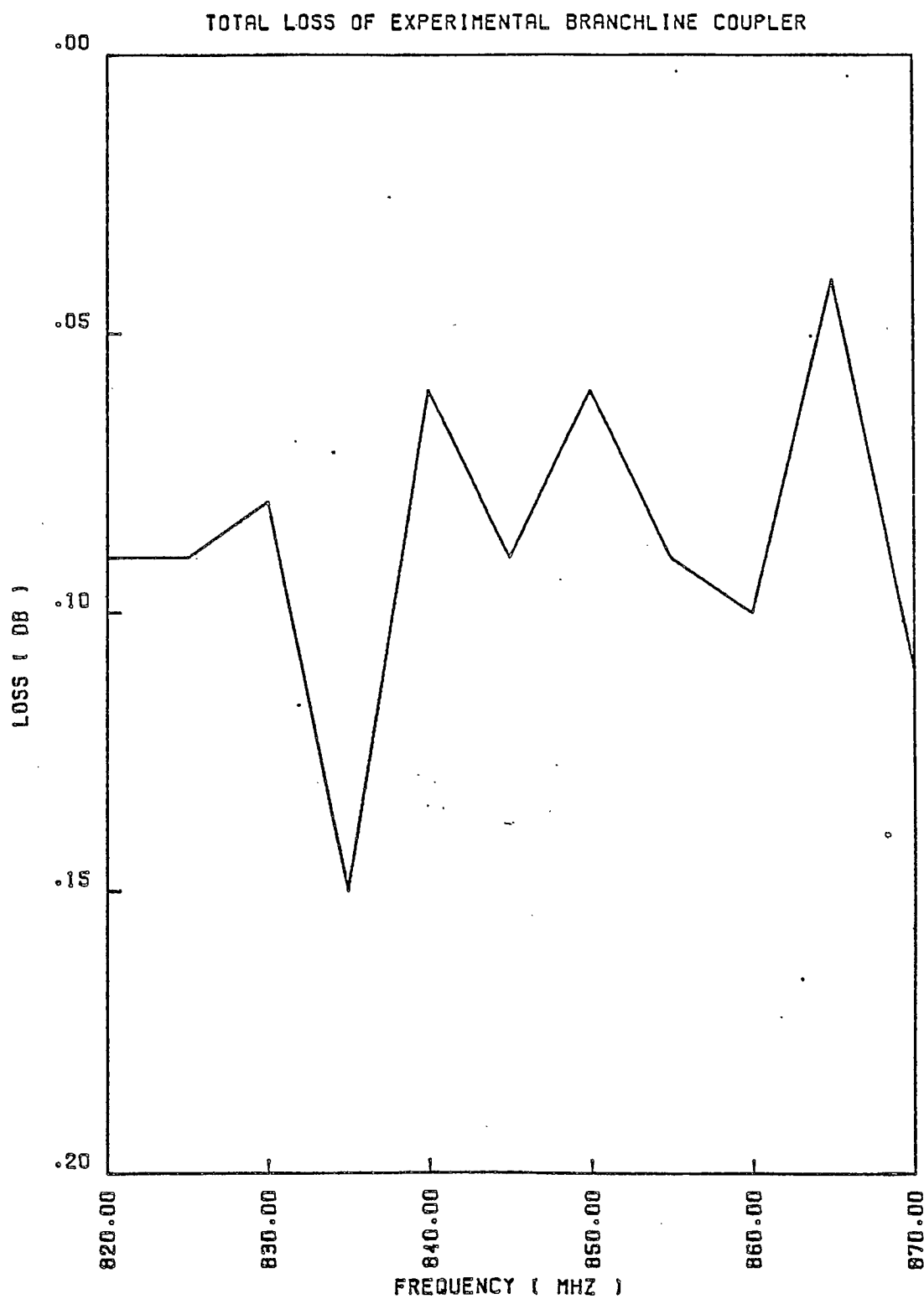


FIGURE 4.5: TOTAL LOSS OF EXPERIMENTAL STRIPLINE COUPLER


For power levels such as proposed for MSAT multipactor breakdown is a real possibility. For this reason, and also to obtain lower loss, it is probable that in general a larger ground plane spacing than the 0.262 inch used experimentally is preferable. Doubling this dimension leads to breakdown powers of about 450W and a halving of the loss. A coupler loss of about 0.05 dB should be achievable. Further increases in dimensions, however, would lead to intolerably wide striplines, large mismatches at transitions between layers and substantially increased mass. If higher power handling capability is required the higher loss of stripline with dielectric such as Teflon or glass/Teflon circuit board materials may be difficult to avoid. The use of low density, low permittivity materials such as space shuttle tile should be investigated.

The power dissipated in the stripline components at MSAT power levels will be significant, primarily because the stripline geometry provides a poor thermal path from the strip to the ground planes. This problem is common to microstrip, squarax and coaxial cables. It may be necessary to provide special heat sinking devices, such as shorted quarter wave stubs shunting the line.

The possible generation of PIM in the BFN components should be investigated. The primary candidates for PIM generation are the pins for suppression of the parallel-plate waveguide mode, connections between layers of the BFN/feed assembly and connections within a layer of the BFN.

It will be necessary to consider power dividers other than the two-branch branchline hybrid, for cases where smaller size or higher performance are required. Reactive power dividers, Wilkinson hybrids, rat-race and 3-branch branchline couplers may be useful and can be implemented in stripline. Coupled-line types may also be useful but care must be taken not to cause

multipactor breakdown between lines in close proximity. It is likely that a mixture of types would be optimum.

|                  |      |  |
|------------------|------|--|
| DOCUMENT No.     | REV. |  <b>COM DEV</b> |
| TDE/MST/2500/001 | —    |  |
|                  |      | SHEET 58   |

## 5.0 DESCRIPTION OF ENGINEERING MODEL

### 5.1 Construction

An engineering model antenna was designed and fabricated to be representative of a single stacked patch element that could make up part of the flight version of an array. This model includes a stacked patch radiator fed from a stripline coupler, making up a module that could be repeated across the array. Also included is an additional layer representing a portion of a beam-forming network fabricated with the antenna array in an integrated panel. An exploded view of the engineering model is illustrated in Figure 5.1

The approximately equal upper and lower patch elements are 0.02 in. thick silver plated aluminum square sheet. They are mounted using five glass fibre rods. The rods have a head at one end and pass through the antenna assembly from the back face. An insulated stainless steel spring washer between the head of each rod and the antenna rear ground plane stiffening structure ensure positive location of the patches over temperature. The rods pass through the patches with four near the corners and one at the centre. Each rod is secured above the upper patch using a glass fibre collar with an aluminum pin pushed through a hole in the collar and dielectric rod. To maintain the required spacing between patches and ground planes the support pins pass through glass fibre tubes. At the centre location between the two patches the support pin passes through an aluminum tube which is bonded with a silver loaded epoxy to the upper and lower patches. This provides a charge leak and a thermally conductive coupling between patches.





TABLE 5.1: ENGINEERING MODEL RETURN LOSS AND  
ISOLATION SUMMARY

|                           | Return Loss (dB) |               | Isolation Between<br>CP Ports (dB) |
|---------------------------|------------------|---------------|------------------------------------|
|                           | <u>Port 1</u>    | <u>Port 2</u> |                                    |
| Without thermal allowance |                  |               |                                    |
| 821-825 MHz               | 20.6             | 17.5          | 15.3                               |
| 866-870 MHz               | 21.0             | 16.6          | 24.0                               |
| With thermal allowance    |                  |               |                                    |
| 819-827 MHz               | 20.4             | 17.4          | 15.0                               |
| 864-872 MHz               | 20.2             | 16.4          | 23.7                               |



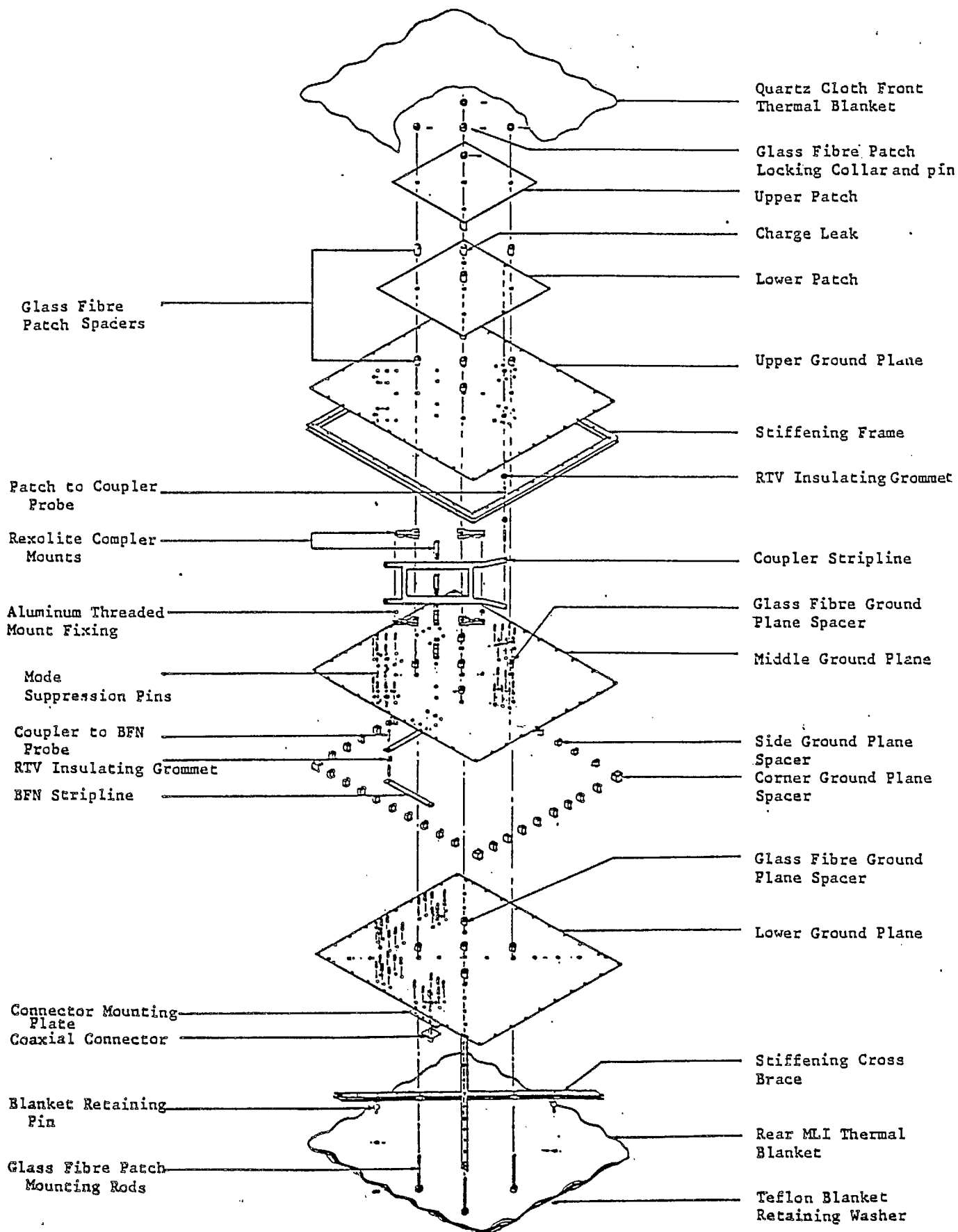


FIGURE 5.1: ENGINEERING MODEL  
EXPLODED VIEW

© Her Majesty the Queen in Right of Canada (1986) as represented by the Minister of Supply And Services.

DOCUMENT No.

TDE/MST/2500/001

REV.



COM DEV

SHEET 61

The structure of the engineering model comprises three ground plane layers of 0.02 in. aluminum sheet of dimensions 12 in. x 10.4 in. spaced apart by an aluminum frame at the coupler level and individual spacers at the BFN layer. The ground planes and spacers have chemical film finish.

Two probes connected to the lower patch pass through holes in the upper ground plane to be attached to the coupler below. Electrical connection to the patch is made by a combination of a 0-80 screw tapped into the end of the probe and solder. The probes are attached to the coupler by TIG welding. The two probes between the coupler and BFN pass through the middle ground plane and are soldered to the coupler and TIG welded to the BFN stripline. Where the probes pass through the ground planes electrical insulation is provided by RTV grommets. The BFN and coupler striplines with their welded probes are silver plated as separate assemblies.

The coupler is machined from a sheet of aluminum and has thickness of 0.062 in. The arms that carry the patch probes are angled through 20° to accommodate the patch attachment locations.

The BFN layer is represented by two 3.2 in. lengths of stripline machined from aluminum sheet to a thickness of 0.062 in.

Each probe connection has six or seven aluminum mode suppression pins around it which are fastened between the ground planes with a 0-80 flat head screw at each end.

The coupler is held at four locations between an upper and lower machined rexolite block. At two of the locations the blocks are attached with 0-80 flat head screws at either end. The screws are countersunk into the ground planes and pass through the ends of the blocks to tap into small aluminum blocks. The remaining two coupler mounts use a 0-80 screw at one end while the other

end is held by a fibre glass patch mounting rod that passes through the antenna.

Each of the two BFN strips are held near their centre by rexolite blocks with 0-80 screws at either end.

The aluminum frame that connects the upper and middle ground planes together around their perimeter comprises four weight relieved lengths of aluminum which are TIG welded at the corners. Each side of the frame is machined to an "I" section with 0.03 in. web and 0.06 in. upper and lower flanges. The cross brace structure on the antenna back face is assembled from two machined "I" section lengths welded at their centre to form an 'X'. To ensure accuracy of the weld configuration both the frame and cross brace are welded while held in a machined aluminum jig.

The upper ground plane is bolted to the frame with 38 x 0-80 flat head screws which are countersunk into the ground plane, to provide a flush surface, and tapped into the frame. The middle and rear ground planes are secured with 38 x 0-80 socket head bolts. Each bolt passes through the rear ground planes, an aluminum spacer, the middle ground plane and taps into the rear side of the frame. The frame and the lower to middle ground plane spacers extend beyond the 12 in. x 10.4 in. ground plane perimeter to allow attachment of adjacent patch antenna modules.

Each of the BFN strips are terminated at a coaxial connector. The central conductor pin is soldered to the BFN strip. The connectors are mounted on aluminum stiffening plates bolted to the rear ground plane.

To allow for attachment of the rear thermal MLI blanket there are four glass fibre blanket support pins. After punching four holes in the blanket they will be pushed over the pins and secured with teflon washers. In order to hold the front thermal blanket clear



of the patches four of the glass fibre rods extend well beyond the patches.

Figure 5.2 is a photograph of the engineering model during assembly with the layer of stripline representing the BFN exposed. In Figure 5.3 the middle ground plane has been added and the circular polarization producing coupler stripline is in place. Figure 5.4 includes the top ground plane. Figure 5.5 shows the completed antenna. Figures 5.6 and 5.7 show it mounted in an extended ground plane used for testing.

## 5.2 RF Performance

For all tests the engineering model antenna was mounted in the centre of a 24 inch square ground plane. Figures 5.8 and 5.9 show the return losses and isolations between input ports measured with input to Port 1 (LHCP) and Port 2 (RHCP) respectively. The data is summarized in Table 5.1. The differences in the two return loss curves appear to be caused by some residual asymmetry in the fabrication. The rather low isolation at the lower end of the frequency range is a combination of the coupler isolation level and the coupling between the feed probes of the antenna itself. The E- and H-plane radiation patterns for each input port at 823 MHz and 868 MHz are shown in Figure 5.10 through 5.13. These were measured with a linearly polarized source horn defining the plane of the E-vector. The beamwidths and squints are summarized in Table 5.2, along with measured axial ratios. The unexpectedly poor axial ratio can be largely attributed to the effect of the inter-probe coupling. The coupling level (about -20 dB at -90 degrees phase) is such as to add directly in phase to the excitation of one linear polarization and to subtract from the other. Using this average value for the coupling an axial ratio contribution of 1.74 dB can be explained. In order to reduce the axial ratio to usable levels it is proposed that a coupler with

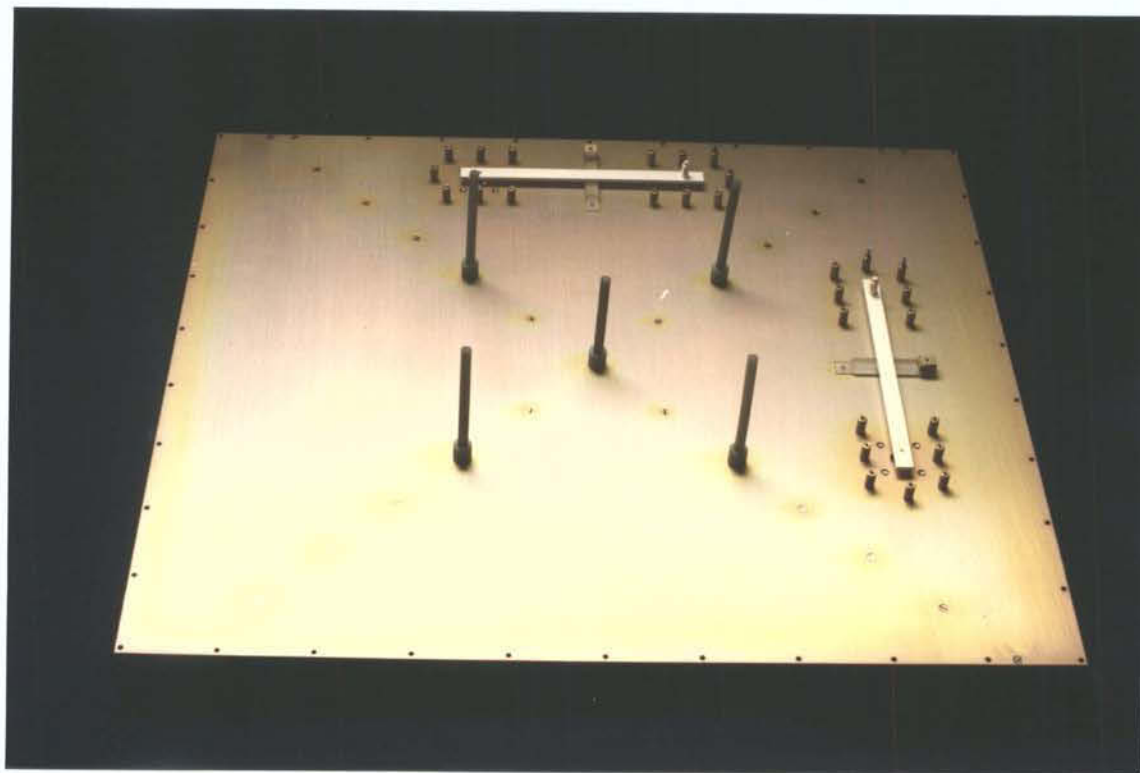


FIGURE 5.2: PHOTOGRAPH OF ENGINEERING MODEL DURING ASSEMBLY  
SHOWING BFN LAYER

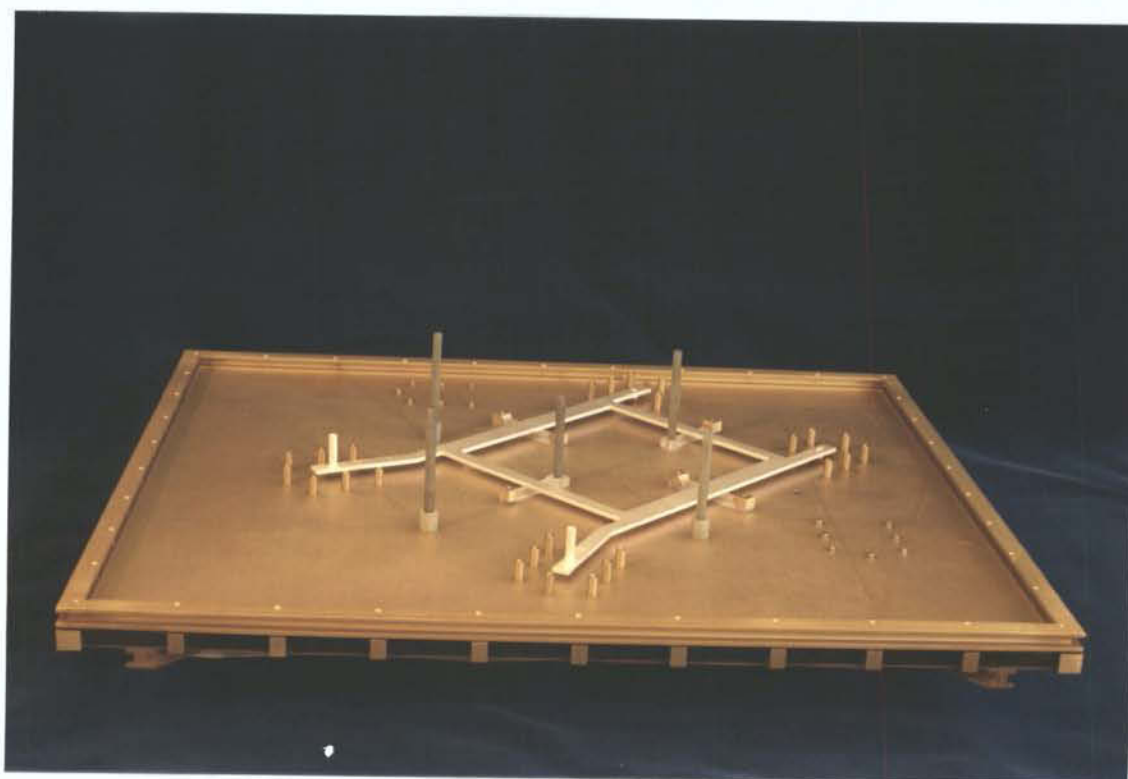


FIGURE 5.3: PHOTOGRAPH OF ENGINEERING MODEL DURING ASSEMBLY  
SHOWING COUPLER LAYER

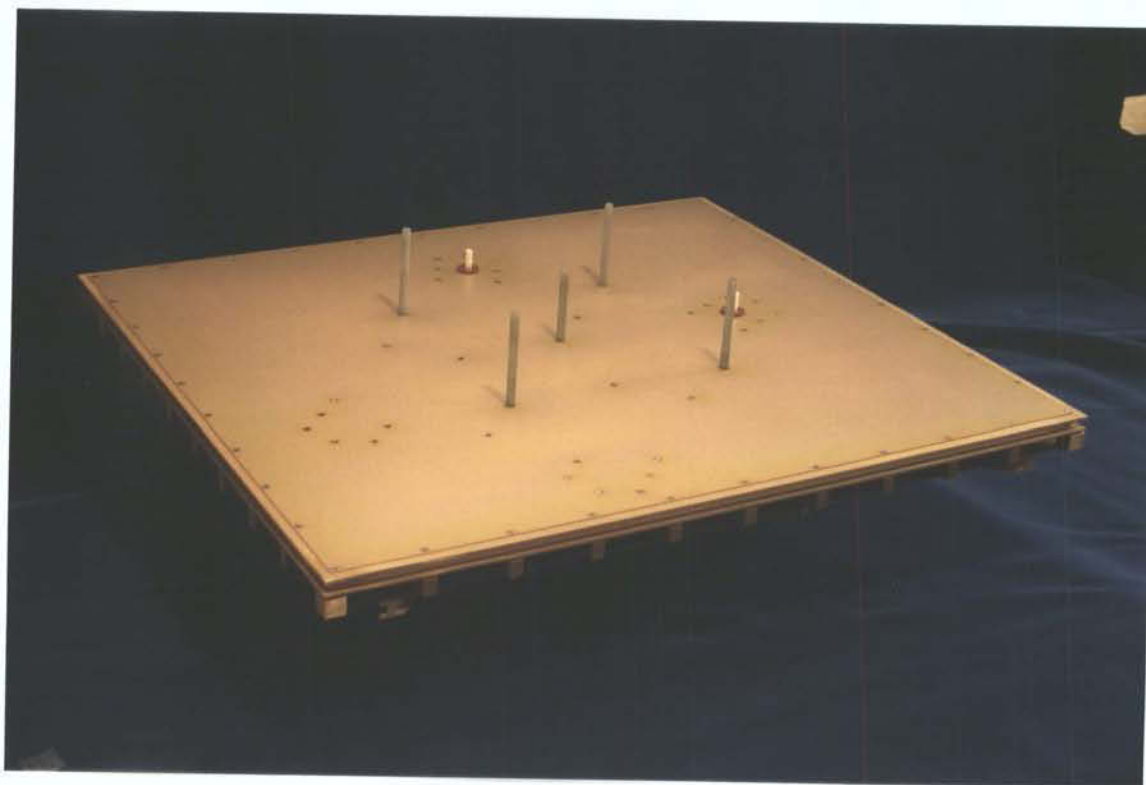


FIGURE 5.4: PHOTOGRAPH OF ENGINEERING MODEL BEFORE PATCH ASSEMBLY



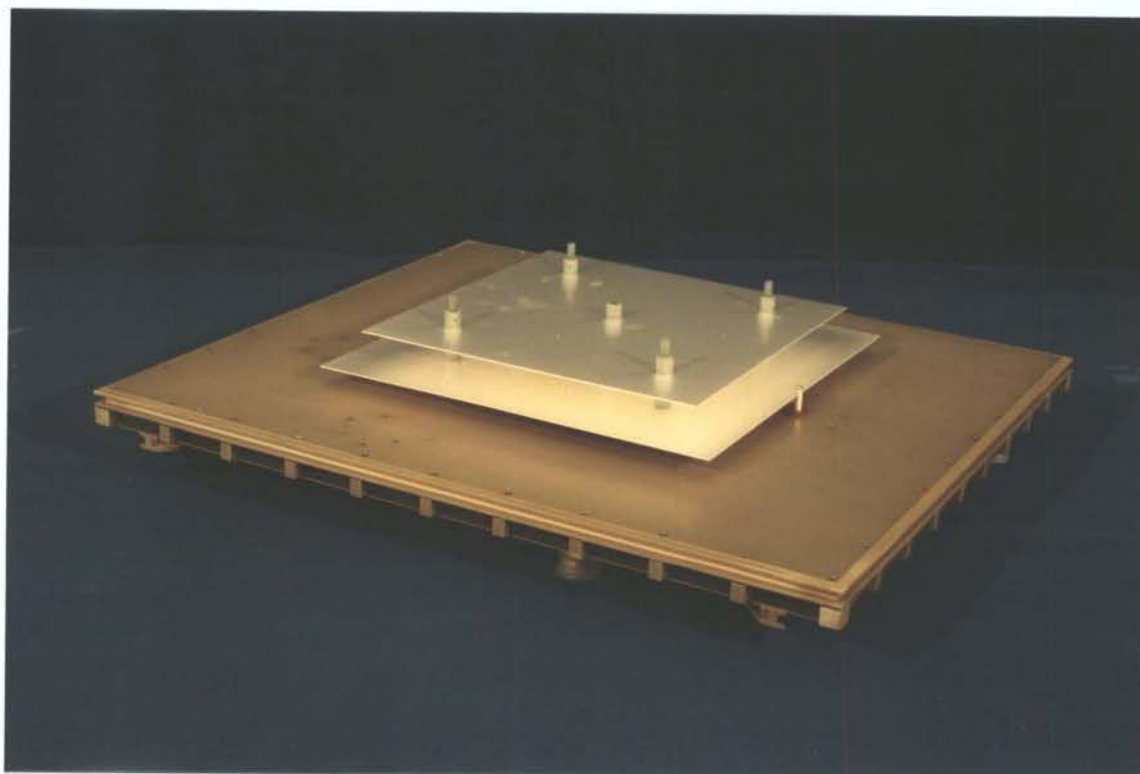


FIGURE 5.5: COMPLETED ENGINEERING MODEL

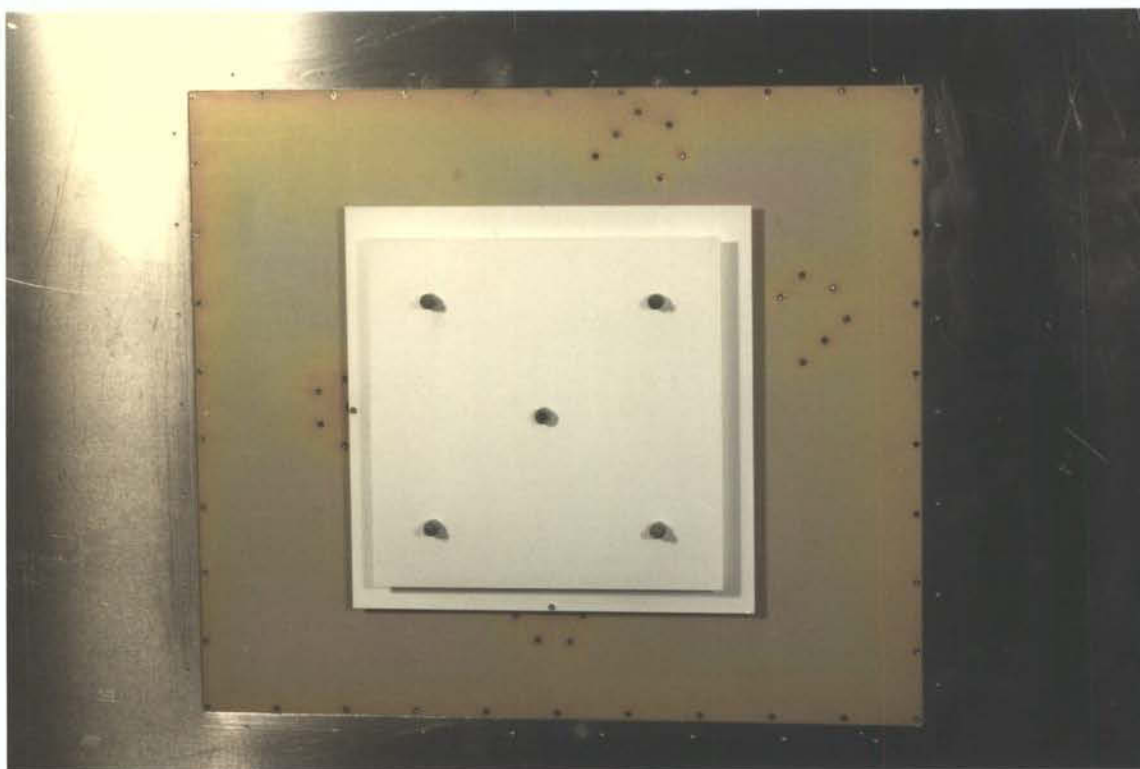


FIGURE 5.6: FRONT FACE OF COMPLETED ENGINEERING MODEL MOUNTED  
IN GROUND PLANE EXTENSION

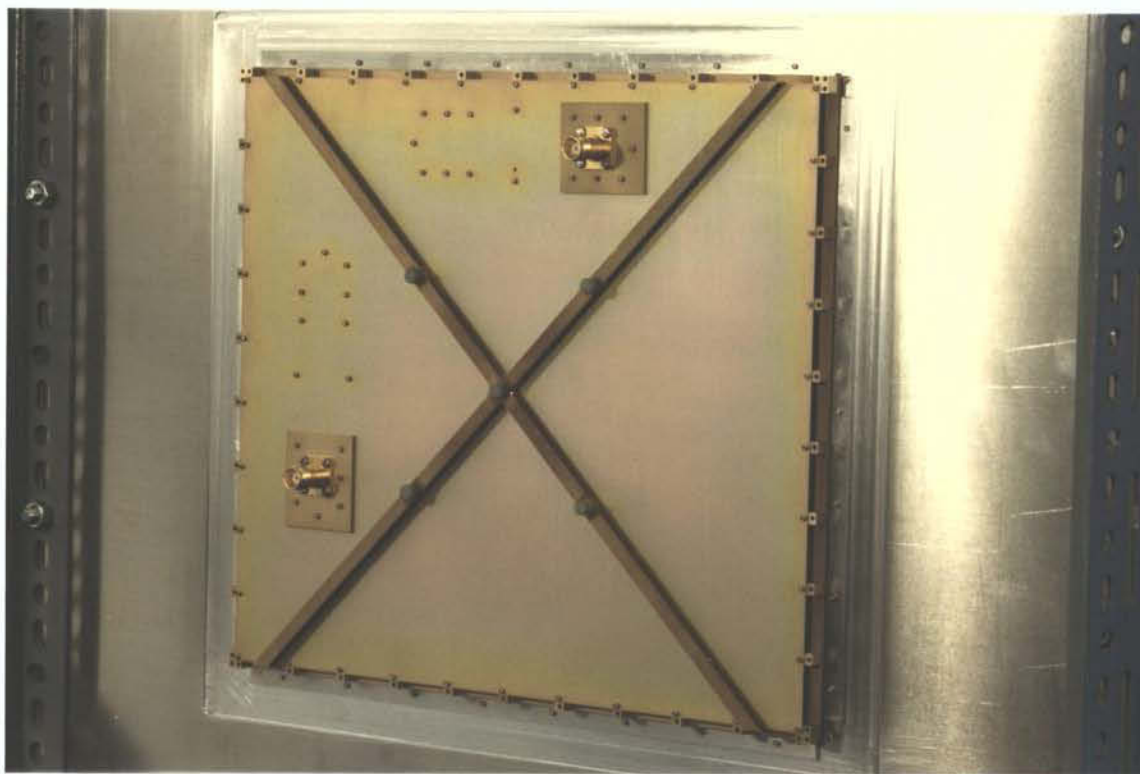


FIGURE 5.7: BACK FACE OF COMPLETED ENGINEERING MODEL MOUNTED  
IN GROUND PLANE EXTENSION



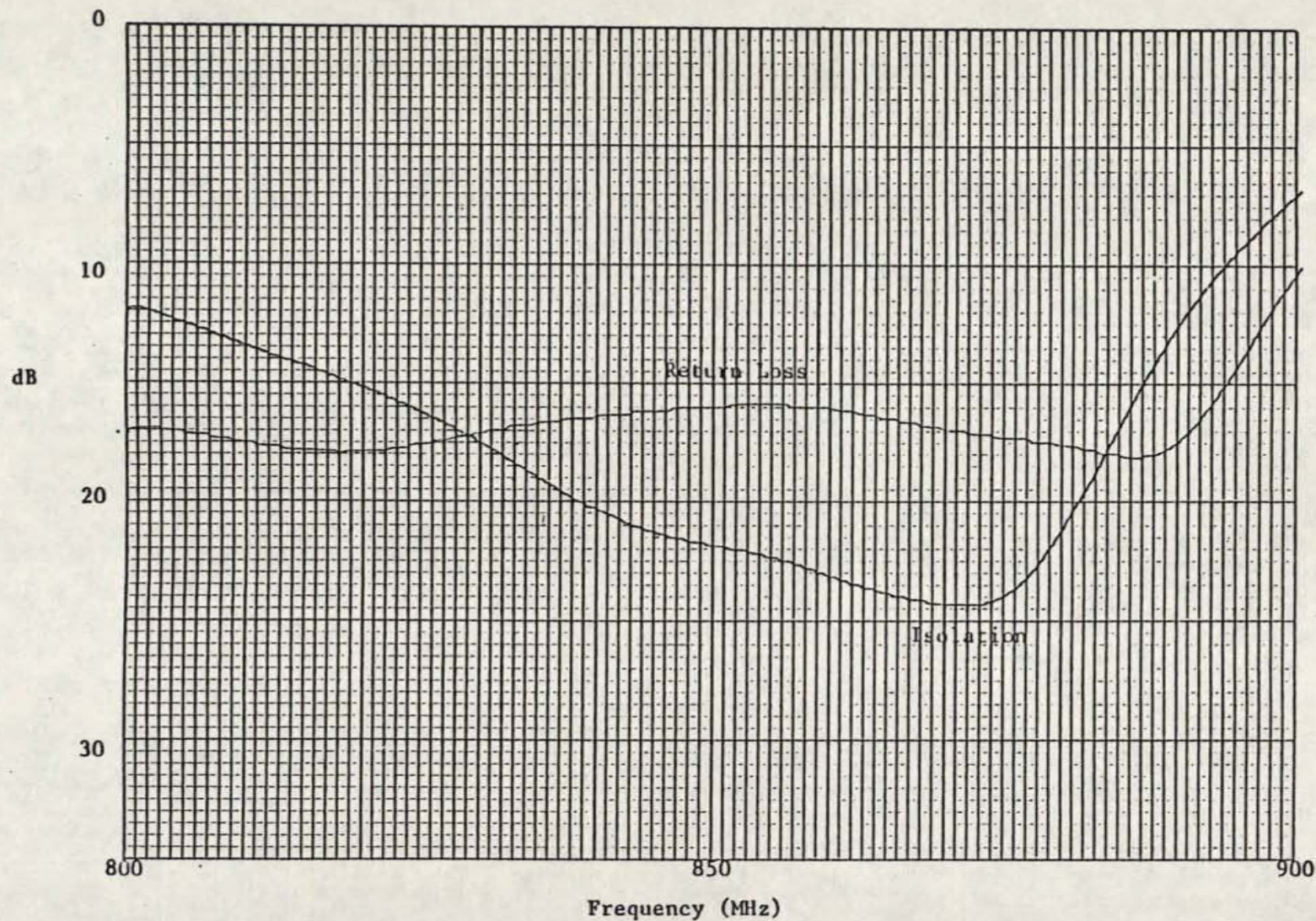


FIGURE 5.9: RETURN LOSS AND ISOLATION OF ENGINEERING MODEL ELEMENT  
(INPUT TO PORT 2)

DOCUMENT No.

TDE/MST/2500/001

REV.

—



COM DEV

SHEET

73



|                  |      |                     |
|------------------|------|---------------------|
| DOCUMENT No.     | REV. | COM DEV<br>SHEET 73 |
| TDE/MST/2500/001 | —    |                     |

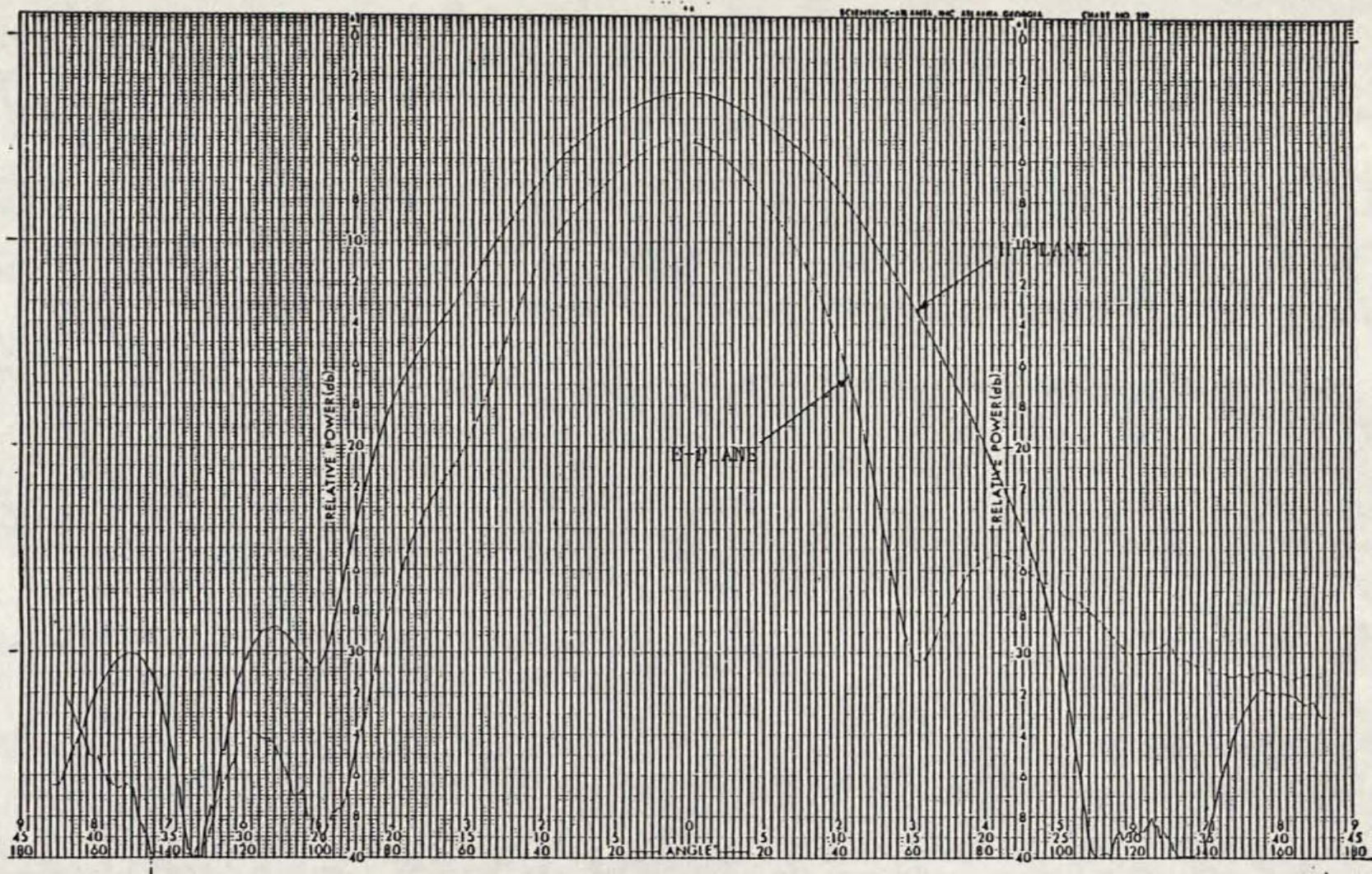


FIGURE 5.10: E- AND H-PLANE PATTERNS OF ENGINEERING MODEL ELEMENT AT 823 MHz (PORT 1)



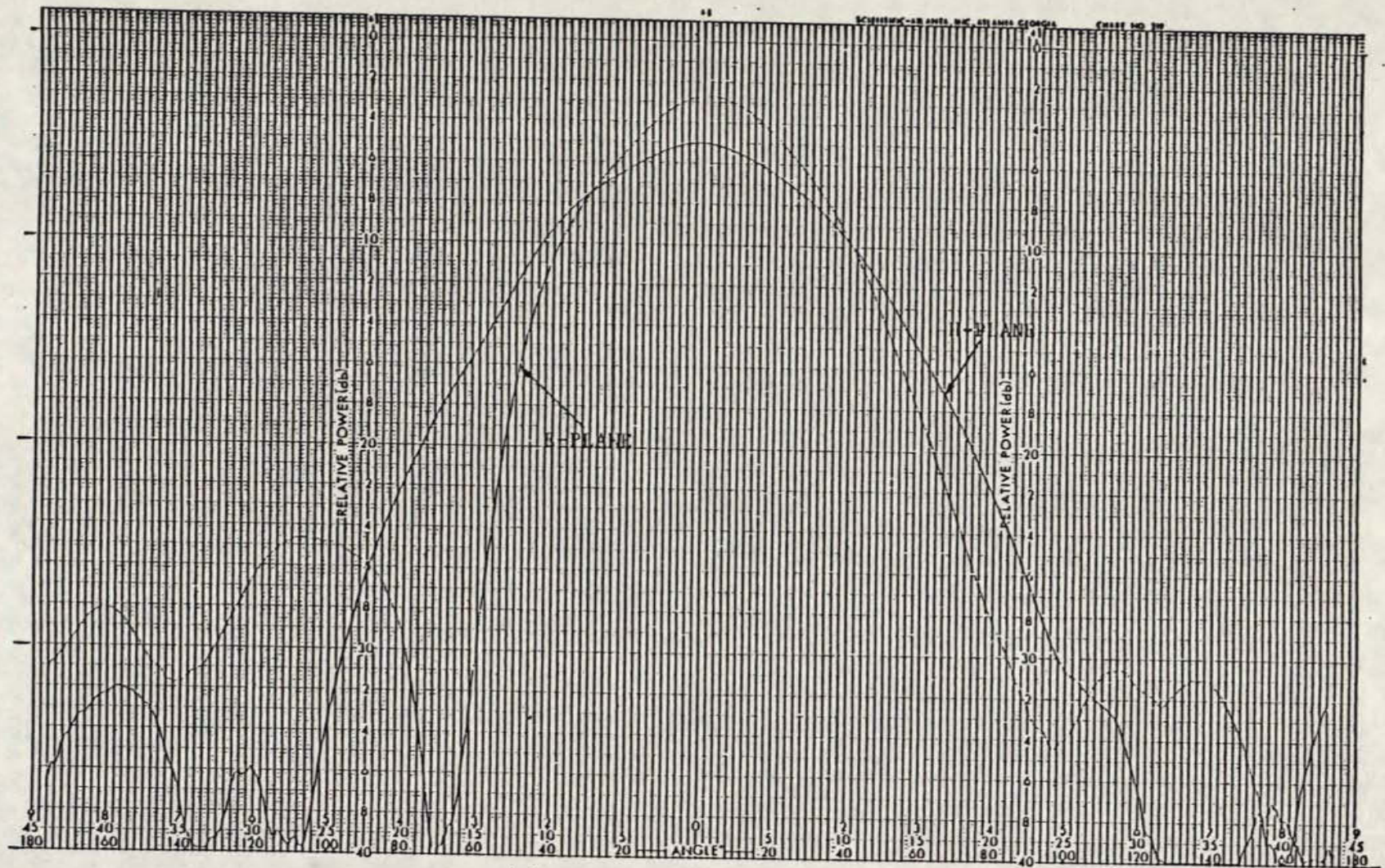


FIGURE 5.11: E- AND H-PLANE PATTERNS OF ENGINEERING MODEL ELEMENT  
AT 823 MHz (PORT 2)

DOCUMENT NO.

REV.

TDE/MST/2500/001



COM DEV

SHEET

74



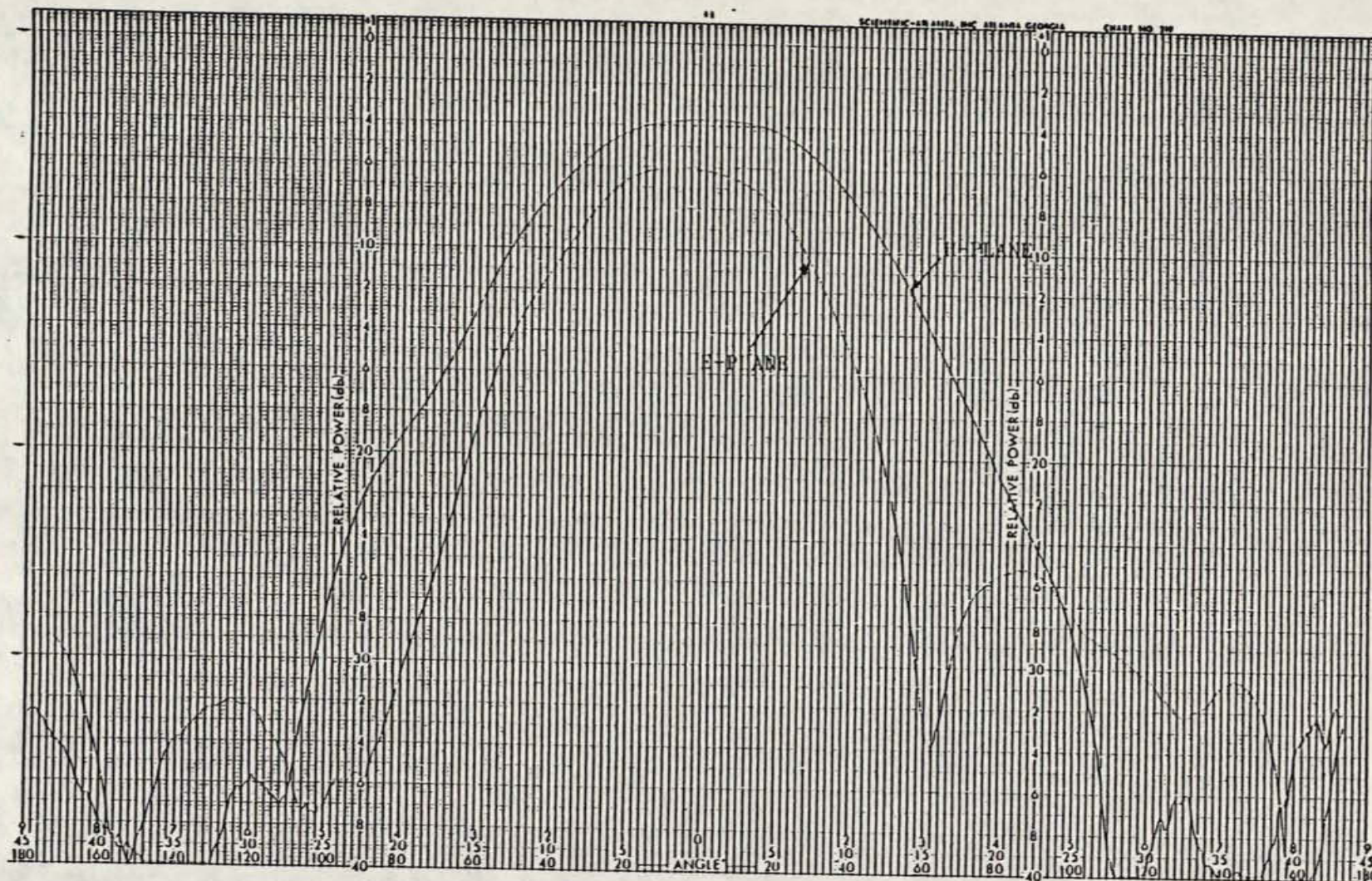


FIGURE 5.12: E- AND H-PLANE PATTERNS OF ENGINEERING MODEL ELEMENT AT 868 MHz (PORT 1)

DOCUMENT No.

REV.

TDE/MST/2500/001

**COM DEV**  
SHEET 75



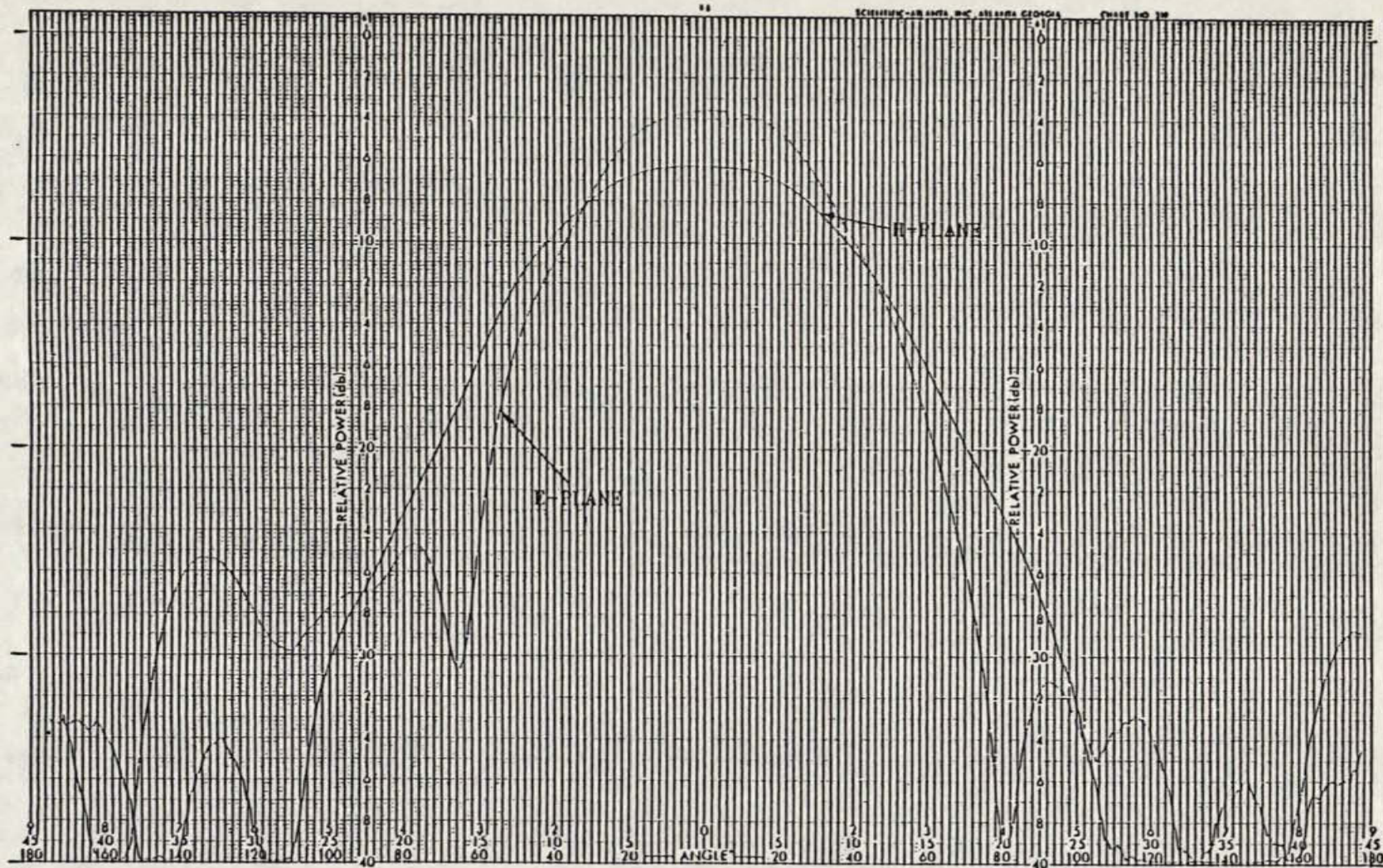


FIGURE 5.13: E- AND H-PLANE PATTERNS OF ENGINEERING MODEL ELEMENT AT 868 MHz (PORT 2)

DOCUMENT No.

REV.

TDE/MST/2500/001


  
COM DEV

SHEET

76

unequal power split be used to counterbalance the effect of the coupling between the feed probes. From the return loss curves it appears that there is some residual asymmetry which may also contribute to the axial ratio. It has been shown that it is possible to achieve 1 dB axial ratio over a good bandwidth using notches in the sides of two-feed patches. It is expected that a very considerable improvement can be achieved using one or more of these techniques. Also included in Table 5.2 are average values of gain, measured by comparison with a standard gain horn. The values of 9.0 - 10.0 dBi are in agreement with published values for single patches.


|                  |      |  |
|------------------|------|--|
| DOCUMENT No.     | REV. |  <b>COM DEV</b> |
| TDE/MST/2500/001 | —    |  |
| SHEET            |      | 77   |



TABLE 5.2: ENGINEERING MODEL PATTERN SUMMARY

|                 | Beamwidth (degrees) |                | Axial Ratio<br>(db) | Gain<br>(db) |
|-----------------|---------------------|----------------|---------------------|--------------|
|                 | <u>E-Plane</u>      | <u>H-Plane</u> |                     |              |
| Port 1, 823 MHz | 47                  | 64             | 2.6                 | 9.2          |
| Port 1, 868 MHz | 57                  | 73             | 2.6                 | 10.0         |
| Port 2, 823 MHz | 48                  | 65             | 2.3                 | 9.0          |
| Port 2, 868 MHz | 57                  | 73             | 2.7                 | 9.7          |

CONCLUSION

In this study the feasibility of using microstrip array antennas and feeds for the MSAT spacecraft at UHF has been investigated. Technology development has been carried out to show the practicality of such antennas and the areas where further development is required for manufacture of a flight antenna have been identified.

Direct radiating microstrip arrays appear to be unsatisfactory for MSAT. Using the construction technique developed during this study, which can handle transmit power with low loss high level beam forming, the estimated mass for a 2-beam array is 160 kg, not including deployment and mounting structures. This is considerably more than would be expected for a wire mesh construction reflector system. In an array there must be continuous ground planes of solid metal to avoid leakage between layers of the beam-formers. As well, there is considerable mass in the extensive BFN's. The large transverse dimensions (at least 4 m, although only about 8cm thick) will probably require the array to be deployed, with the associated problems of high power, low PIM RF motional joints. A four beam array will require active transmit/receive modules at the subarray level, and low level beam forming. Deployment would be difficult as the overall size would be near 4 by 8 metres.


On the other hand, the use of microstrip antennas in the feed array for a reflector is quite feasible and can offer some advantages over conventional horns. Prior to this study the essential obstacle to the use of microstrip antenna techniques for transmit/receive feeds for MSAT has been bandwidth. However, with development of stacked patch antennas this is no longer a



problem. As part of this project such elements were constructed which meet a specification of 20 dB return loss over both transmit and receive bands of MSAT, with radiation patterns that change very slowly with frequency. While good axial ratio has not yet been achieved it appears that it will not be difficult to obtain with minor changes to the feed system of the engineering model. Mutual coupling measurements carried out during this study will permit the prediction of the performance of an array of these elements.


The thickness of such an array has been estimated at 6.6 cm, including thermal blankets on both surfaces, although this might have to be increased (perhaps to 8 cm) to improve power ratings. A 2-beam feed array will have transverse dimensions of 1.14 by 1.52 metres and a mass of 10.9 kg while a 4-beam feed measures 1.68 by 1.98 m with a mass of 20.9 kg. These designs are conservative in the sense that the element spacing has been chosen to keep mutual coupling effects to a minimum. The sizes may be reduced with careful design including mutual coupling effects. This could permit a reduction in reflector  $f/D$  from the assumed value of 0.85 required by these feeds. Simplification of the feeds (especially the two-beam version) could also reduce the feed size and reflector  $f/D$  while allowing less control of sidelobes than possible with full septet feeds. The estimated in-service temperature range that would be seen by these arrays is  $-90^{\circ}\text{C}$  to  $+50^{\circ}\text{C}$ . Performance of an antenna system will be similar to that with horn feeds, but with a lighter feed which is more easily stowable because of its reduced thickness.

A number of critical areas have been identified which require resolution or offer possible improved characteristics. Initially the axial ratio of the engineering model should be improved.

|                  |      |  |
|------------------|------|--|
| DOCUMENT No.     | REV. |  <b>COM DEV</b> |
| TDE/MST/2500/001 | —    |  |
| SHEET            |      | 80   |

Construction techniques should be examined further including the possible use of copper clad dielectric honeycomb as a patch antenna substrate and aluminum honeycomb as antenna array stiffening on the back face. Fastening methods should be considered to reduce the number of screw junctions, in part to minimize passive intermodulation. Identification of suitable materials for space applications must be considered in more detail, particularly with respect to low temperature, low loss dielectrics and the front face thermal blanket. Further work on quantification of power carrying ability of the components will be required. Multipactor discharge, PIM and power dissipation will all be significant factors in design but none are expected to prohibit operation at MSAT power levels. There is potential for improvement of the stacked patch element. Theoretical modelling of such antennas with accurate methods would be useful. A comparison of circular and square patches should be made, with regard to bandwidth, return loss and mutual coupling. If a suitable 4-phase power divider can be found a four feed element should be considered to improve axial ratio.

The patch array feed concept offers equivalent performance to conventional horn arrays with the advantage of lower volume and competitive mass. With further optimization of the engineering model design, volume and mass reduction is feasible and a fully space-qualifiable technology will be developed.

|                  |      |  |
|------------------|------|--|
| DOCUMENT No.     | REV. |  <b>COM DEV</b> |
| TDE/MST/2500/001 | —    |  |
|                  |      | SHEET 81   |



P91 .C654 D49 1986 Summ.

[illegible]

INDUSTRY CANADA / INDUSTRIE CANADIENNE

208057



**COM DEV PRODUCTS AND SERVICES  
FOR  
COMMUNICATIONS AND RADAR SYSTEMS**

**HIGH POWER MICROWAVE PRODUCTS**

- High Power Filters, Diplexers, Combiners
- High Power Isolators, Circulators
- High Power Couplers, Splitters, Terminations
- Low Loss Transmit Reject Filters
- Variable Power Combiners
- High Power Antenna Co-polarized Diplexers
- Amplitude Equalizers
- Group Delay Equalizers

**COMMUNICATIONS SATELLITE PRODUCTS**

- Low Loss, High Order Dual Mode Output Multiplexers
- Beam Switching and Beam Reconfiguring Networks
- High Power Microwave Components and Subsystems
- Waveguide and Coax Isolators, Circulators
- Low Pass Receive Band and Harmonic Band Reject Filters
- Low Loss Preselect Filters
- Group Delay and Amplitude Equalized Input Multiplexers
- Waveguide to SMA Adaptors and Monitor Couplers
- Telemetry and Command Filters
- Variable Power Dividers

**CONSULTING SERVICES**

- Conceptual, hardware and systems of Microwave transponders and Communications Subsystems for Communications Satellites.
- Tradeoff analyses, layout and hardware design of high power combining and multiplexing networks for Satellite Earth Terminals.
- All software and hardware aspects of devices and subsystems involving microwave filtering networks and ferrite devices for both terrestrial and satellite communications systems.



**COM DEV LTD.**

MICROWAVE DEVICES AND SUBSYSTEMS FOR TERRESTRIAL AND SATELLITE COMMUNICATIONS

155 SHELDON DRIVE,  
CAMBRIDGE, ONTARIO, CANADA N1R 7H6  
TEL.: (519) 622-2300 • TWX: 610-366-3164